

This article is published as part of the *Dalton Transactions* themed issue entitled:

Dalton Transactions 40th Anniversary

Guest Editor Professor Chris Orvig, Editorial Board Chair
University of British Columbia, Canada

Published in issue 40, 2011 of *Dalton Transactions*

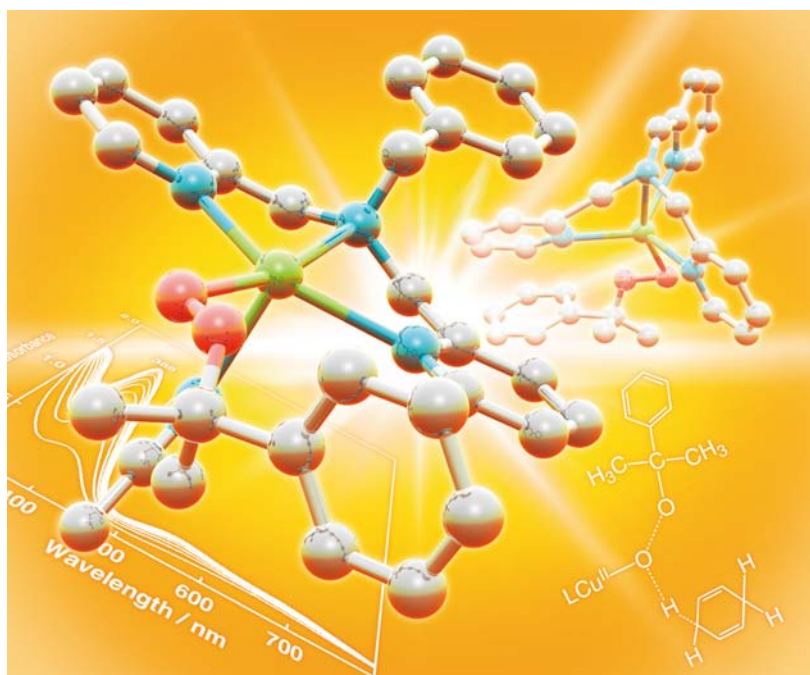


Image reproduced with permission of Shinobu Itoh

Welcome to issue 40 of the 40th volume of *Dalton Transactions*-40/40! Articles in the issue include:

PERSPECTIVE:

[Synthesis and coordination chemistry of macrocyclic ligands featuring NHC donor groups](#)

Peter G. Edwards and F. Ekkehardt Hahn
Dalton Trans., 2011, 10.1039/C1DT10864F

FRONTIER:

[The future of metal–organic frameworks](#)

Neil R. Champness
Dalton Trans., 2011, DOI: 10.1039/C1DT11184A

ARTICLES:

[Redox reactivity of photogenerated osmium\(II\) complexes](#)

Jillian L. Dempsey, Jay R. Winkler and Harry B. Gray
Dalton Trans., 2011, DOI: 10.1039/C1DT11138H

[Molecular squares, cubes and chains from self-assembly of bis-bidentate bridging ligands with transition metal dications](#)

Andrew Stephenson and Michael D. Ward
Dalton Trans., 2011, DOI: 10.1039/C1DT10263J

Visit the *Dalton Transactions* website for more cutting-edge inorganic and organometallic research

www.rsc.org/dalton

Cite this: *Dalton Trans.*, 2011, **40**, 10513

www.rsc.org/dalton

PAPER

Indenyl ring slippage in crown thioether complexes $[\text{IndMo}(\text{CO})_2\text{L}]^+$ and C–S activation of trithiacyclononane: Experimental and theoretical studies†

Carla A. Gamelas,^{a,b} Nuno A. G. Bandeira,^c Cláudia C. L. Pereira,^a Maria José Calhorda,^c Eberhardt Herdtweck,^d Miguel Machuqueiro,^c Carlos C. Romão^a and Luís F. Veiros^e

Received 8th April 2011, Accepted 21st June 2011

DOI: 10.1039/c1dt10607d

The macrocycle 1,4,7-trithiacyclononane (ttcn) reacts with $[(\eta^5\text{-Ind})\text{Mo}(\text{CO})_2(\text{NCMe})_2]^+$ (or $[(\eta^5\text{-Ind})\text{Mo}(\text{CO})_2(\kappa^2\text{-dme})]^+$) to give $[(\eta^3\text{-Ind})\text{Mo}(\text{CO})_2(\kappa^3\text{-ttcn})]^+$ as the BF_4^- salt (**1**), but its reaction with $[(\eta^5\text{-Ind})\text{Mo}(\text{CO})_2(\text{C}_3\text{H}_6)(\text{FBF}_3)]$ affords the C–S bond cleavage product $[(\eta^5\text{-Ind})\text{Mo}(\text{CO})_2(\kappa^3\text{-1,4,7-trithiaheptanate})]\text{BF}_4$ (**6**), which has been characterised by X-ray crystallography (Ind = C_9H_7 , indenyl). In contrast to ttcn, the macrocycles 1,3,5-trithiane (tt) and 1,4,7,10-tetrathiacyclododecane (ttcd) fail to induce changes in the coordination mode of indenyl: tt and ttcd react with $[(\eta^5\text{-Ind})\text{Mo}(\text{CO})_2(\text{NCMe})_2]^+$ (or $[(\eta^5\text{-Ind})\text{Mo}(\text{CO})_2(\kappa^2\text{-dme})]^+$) to give $[(\eta^5\text{-Ind})\text{Mo}(\text{CO})_2(\kappa^2\text{-tt})]^+$ (**2**), characterised by X-ray crystallography, and $[(\eta^5\text{-Ind})\text{Mo}(\text{CO})_2(\kappa^2\text{-ttcd})]^+$ (**3**), respectively. The cyclopentadienyl (Cp = C_5H_5) analogues $[(\eta^5\text{-CpMo}(\text{CO})_2(\kappa^2\text{-tt})]^+$ (**4**) and $[(\eta^5\text{-CpMo}(\text{CO})_2(\kappa^2\text{-ttcn})]^+$ (**5**) have also been synthesised and **5** characterised by X-ray crystallography. DFT calculations showed that the $\eta^5\text{-Ind/Cp}$ coordination mode is always the most stable. However, a molecular dynamics study of the macrocycles conformations revealed that the major conformer of ttcn was a chair, which favoured κ^3 coordination. As indenyl complexes undergo slippage with a small barrier ($<10 \text{ kcal mol}^{-1}$), the kinetically preferred species $[(\eta^3\text{-Ind})\text{Mo}(\text{CO})_2(\kappa^3\text{-ttcn})]^+$ (**1**) is the observed one. The conversion to **6** proceeds stepwise, with loss of ethylene followed by loss of CO, as calculated by DFT, with a barrier of $38.7 \text{ kcal mol}^{-1}$, consistent with the slow uncatalysed reaction.

Introduction

The capacity of organic π ligands to adjust their hapticity, *i.e.*, the number of metal–C bonds, to the electronic needs of a metal center gives rise to processes known as “ring slippage”, “ring folding”,¹ or, more generally, as “haptotropic shifts”.² Among those ligands, the most popular are certainly cyclopentadienyl (Cp = C_5H_5) and indenyl (Ind = C_9H_7). In particular, the long known^{3–9} substantial increase in the rates of substitution reactions of electronically saturated Ind complexes, when compared to their Cp counterparts, has given rise to the term “indenyl effect”,

coined by Basolo *et al.*⁷ These accelerated rates of reaction of indenyl complexes have found broad application in the catalysis of some important organic reactions, namely cyclotrimerization of alkynes (to form substituted benzenes), co-cyclotrimerization of alkynes and nitriles (to form substituted pyridines),¹⁰ co-cyclization of alkyne, alkene and carbon monoxide (to form cyclopentenones),¹¹ and alkene hydroboration.¹² Furthermore, indenyl¹³ and fluorenyl¹⁴ complexes are of practical use in the olefin polymerization, being much better precursors than their Cp congeners, in terms of yield and stereoregularity.

The indenyl effect has been interpreted in terms of the metal–Cp' bond strength (Cp' = Cp or Ind) in the two relevant hapticity modes: $\eta^5\text{-Cp}'$ and $\eta^3\text{-Cp}'$.¹⁵ On one hand, the M–($\eta^5\text{-Cp}'$) bond is stronger for cyclopentadienyl, providing a ground-state stabilization for the complexes with $\eta^5\text{-Cp}$, when compared to their indenyl analogues. On the other hand, the M–($\eta^3\text{-Cp}'$) bond is stronger for Ind than for Cp, stabilizing the corresponding trihapto intermediates and transition states and, thus, increasing the reaction rate. A list of references on haptotropic shifts, with emphasis on Cp, Ind, and the indenyl effect, can also be found in the same work.¹⁵ The situation becomes more complicated when fluorenyl or larger polycyclic rings are considered.¹⁶ More recent examples on Ind haptotropic shifts are scarce¹⁷ and some of them open new perspectives in organometallic chemistry, namely in the construction of molecular machines.¹⁸ $\eta^3\text{-Ind}$ coordination

^aInstituto de Tecnologia Química e Biológica, da Universidade Nova de Lisboa, Av. da República, EAN, 2780-157, Oeiras, Portugal

^bEscola Superior de Tecnologia, Instituto Politécnico de Setúbal, Vale de Estefanilha, 2910-761, Setúbal, Portugal

^cDepartamento de Química e Bioquímica, Faculdade de Ciências, Universidade de Lisboa, Campo Grande, 1749-016, Lisboa, Portugal

^dLehrstuhl für Anorganische Chemie der Technischen Universität München, Lichtenbergstr., 4, 85747, Garching b, München, Germany

^eCentro de Química Estrutural, DEQB, Instituto Superior Técnico, Universidade Técnica de Lisboa, Av., Rovisco Pais, 1049-001, Lisboa, Portugal

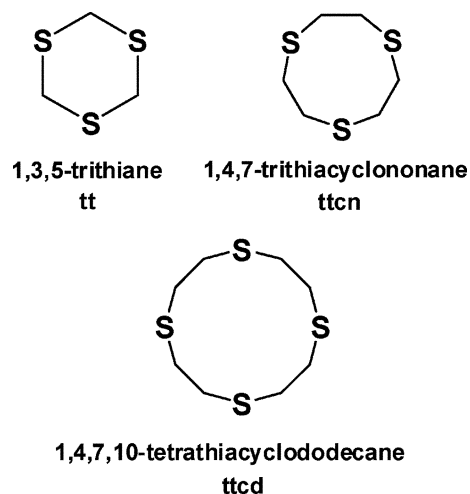
† Electronic supplementary information (ESI) available: Tables of atomic coordinates for all the optimised structures and slippage parameters for **2**, **5** and **6**. CCDC reference numbers 820539 (**2**), 820540 (**5**) and 820541 (**6**). For ESI and crystallographic data in CIF or other electronic format see DOI: 10.1039/c1dt10607d

remains relatively rare in ground-state structures.¹⁹ The indenyl slippage reaction can be induced in organometallic systems by ligand addition (L) or by a two-electron reduction, resulting in a η^5 to η^3 haptotropic migration, or in the reverse direction accompanying ligand elimination or oxidation processes. The η^5 coordination mode is usually very symmetric for Cp with five similar M–C distances, but becomes more asymmetric for Ind, being best described as $\eta^3 + \eta^2$, with three M–C bonds shorter than the other two to the junction carbon atoms. In some cases, an intermediate coordination mode of the indenyl is observed, corresponding to addition of only one electron. It is well observed for $[(\text{Ind})_2\text{Ni}]$ in the series of metallocenes $[(\text{Ind})_2\text{M}]$ for M = Fe, Co, Ni, where the increasing electron count (Fe (18e) < Co (19e) < Ni (20e)) leads to an extra electron in each indenyl ligand of the Ni complex, and intermediate slip and bending parameters.²⁰ This type of intermediate bonding is also observed in the complex $[(\text{Ind})(\text{Cp})\text{Mo}\{\text{P}(\text{OMe})_3\}_2]^+$, a formally 19-electron complex intermediate in the reversible redox pathway between $[(\eta^5\text{-Ind})(\text{Cp})\text{Mo}(\text{PR}_3)_2]^{2+}$ and $[(\eta^3\text{-Ind})(\text{Cp})\text{Mo}(\text{PR}_3)_2]$ ($\text{PR}_3 = 1/2 \text{ dppe}, \text{P}(\text{OMe})_3$).²¹

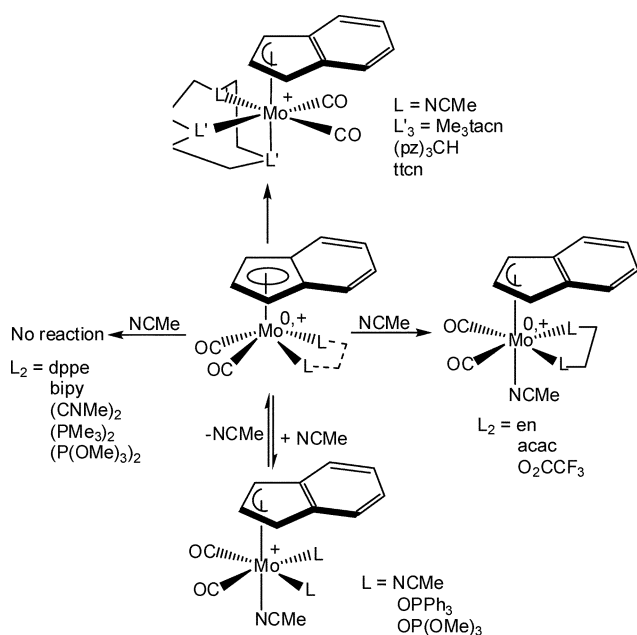
The number of very recent computational studies investigating hapticity rearrangements of Ind,^{22–25} as well as larger π ligands,^{26,27} indicates that this subject remains important. For example, the capability of the indenyl ligand to extend its hapticity to the entire π system, reaching an extraordinary η^9 -Ind coordination mode, was established lately in $[(\text{Ind})_2\text{Zr}]$ sandwich complexes.^{28–30} These species may contribute to explain the existence of an indenyl effect, even in the presence of dissociative mechanisms,³⁰ though other hypotheses must be considered.³¹

Understanding the dependence of the ligand-induced indenyl η^5 to η^3 shift on the nature of the ligand is the starting point of this work. Scheme 1 summarizes our earlier findings on this topic using $[(\eta^5\text{-Ind})\text{Mo}(\text{CO})_2\text{L}_2]^+$ complexes as reaction models.^{32,33} The ring slippage reaction depends strongly on both the incoming and the ancillary ligands (L) present in the initial complex. Besides NCMe, ring slippage is observed in the presence

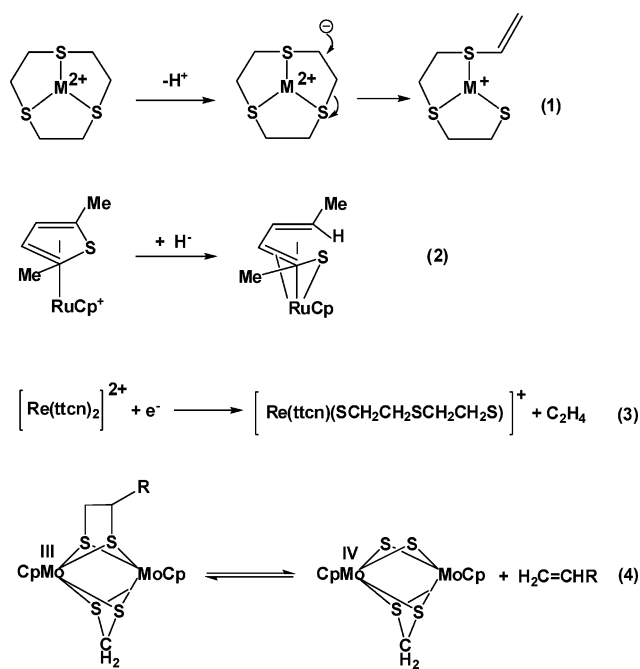
of ethylenediamine (en), oxygen ligands such as acac, O_2CCF_3 , OPPh_3 and $\text{OP}(\text{OMe})_3$, but not with CNMe, phosphanes and bipy (Scheme 1).^{32,33} Computational studies helped to rationalise this behaviour, taking advantage of the contrasting reactivity of NCMe (slippage promoter) and CNMe (slippage inhibitor).³³ Without much surprise, we also found that tridentate ligands such as Me_3tacn (1,4,7-*N,N',N''*-trimethyltriazacyclononane), $(\text{pz})_3\text{CH}$ (tris(pyrazolyl)methane) and ttcn (1,4,7-trithiacyclononane) can also promote Ind ring slippage in the same system.^{32,33} In fact, both electron count and stereochemistry seem appropriate and the chelating effect eventually compelling. Since $[(\eta^3\text{-Ind})\text{Mo}(\text{CO})_2(\kappa^3\text{-ttcn})]^+$ was found to be the only reported molybdenum complex with neutral sulfur ligands and indenyl in a trihapto coordination mode we decided to extend this work to the polythiacycloalkanes in Scheme 2 in search of other examples of these haptotropic shifts. Indeed, both the stereochemistry and the electron count seemed to be readily compatible with a ring-slipped structure of the type $[(\eta^3\text{-Ind})\text{Mo}(\text{CO})_2(\kappa^3\text{-S3})]^+$ ($\text{S3} = \text{tt}, \text{ttcn}$) just as it was found for $\text{S3} = \text{ttcn}$.



Scheme 2



Moreover, the observation that the $[(\eta^3\text{-Ind})\text{Mo}(\text{CO})_2(\kappa^3\text{-ttcn})]^+$ complex was prone to undergo elimination of ethylene and CO to produce the $\text{Mo}(\text{IV})$ complex $[(\eta^3\text{-Ind})\text{Mo}(\kappa^3\text{-1,4,7-trithiaheptanate})(\text{CO})]^+$ in a very clean process, spurred our curiosity on the ring-slipped ttcn complex. In fact, the ring opening of thioether crowns, in particular ttcn, has been the subject of a number of studies where it is usually started by a clear chemical trigger, which was not obvious in our case. In a report directly related to our work, Blower and co-workers found that the chemical or electrochemical reduction of the thioether complex $[\text{Re}^{\text{III}}(\text{ttcn})_2]^{2+}$ leads to ethylene loss with formation of $[\text{Re}^{\text{III}}(\text{ttcn})(\text{SCH}_2\text{CH}_2\text{SCH}_2\text{CH}_2\text{S})]^+$ (eqn (3) in Scheme 3).³⁴ In cationic complexes such as $[\text{M}(\text{ttcn})_3]^{3+}$ ($\text{M} = \text{Co}, \text{Rh}, \text{Ir}$), ethylene loss is initiated by deprotonation at an α -methylene carbon centre, which causes cleavage of an adjacent C–S bond and formation of a chelate vinylthioether–thiolate complex (eqn (1) in Scheme 3).³⁵ Low-valent, electron rich metal complexes promote oxidative addition across the C–S bond, creating a metal thiolate. The observed release of 1-butene during the removal of sulfur from thiophene in the hydrodesulfurization (HDS) process, over CoMoS catalysts, occurs by C–S bond homolysis, after the oxidative addition



step.³⁶ These conditions also promote protonolysis reactions of coordinated ligands followed by homolytic S–C bond cleavage.³⁷

Examples of C–S activation that do not involve direct insertion of the metal into the carbon–heteroatom bond include nucleophilic addition reactions. For example, Angelici *et al.* have shown that the complex $[\text{CpRu}(\eta^5\text{-thiophene})]^+$ undergoes C–S cleavage upon hydride addition to α -carbon *via* an associative mechanism (eqn (2) in Scheme 3).³⁸ Eventually closer to the ethylene extrusion that we observe, are the bridging bis-thiolate complexes with two CpMo centers, where ethylene loss is accompanied by a two-electron oxidation process from Mo(III) to Mo(IV) (eqn (4) in Scheme 3).³⁷ Both the need to explain the reasons for the impaired ring-slippage induction in the cases of the tt and ttcd rings, and to understand whether the indenyl coordination had some responsibility in the control of ethylene extrusion from the ttcn ring, originated the present work. Here the structural chemistry of the $[(\text{Cp}')\text{Mo}(\text{CO})_2(\text{S}3)]^+$ ($\text{Cp}' = \text{C}_5\text{H}_5, \text{C}_9\text{H}_7$; $\text{S}3 = \text{tt}, \text{ttcn}, \text{ttcd}$), as well as the reactivity induced in the $[\text{Cp}'\text{Mo}(\text{CO})_2]^+$ fragment by those sulfur macrocycles, is explored and complemented by a DFT³⁹ mechanistic study that is revealing of the subtle nature of the stereochemical and electronic processes involved in molecules that feature both flexible, labile classical ligands and electronically flexible hydrocarbon ligands.

Chemical studies

Synthesis and characterization of $[\text{Cp}'\text{Mo}(\text{CO})_2\text{L}]^+$ complexes ($\text{Cp}' = \text{Ind}, \text{Cp}$; $\text{L} = \text{tt}, \text{ttcn}, \text{ttcd}$). As previously published, the sulfur macrocycle 1,4,7-trithiacyclononane (tcn) reacts with $[(\eta^5\text{-Ind})\text{Mo}(\text{CO})_2(\text{NCMe})_2]\text{BF}_4$ to give the ring-slipped complex $[(\eta^3\text{-Ind})\text{Mo}(\text{CO})_2(\kappa^3\text{-tcn})]\text{BF}_4$ (**1**) in excellent yield (Scheme 1).³⁵

Hoping to get analogous ring slipped complexes with other polythia macrocycles, the same synthetic method was used with 1,3,5-trithiane (tt) and 1,4,7,10-tetrathiaclododecane (ttcd), affording complexes $[(\eta^5\text{-Ind})\text{Mo}(\text{CO})_2(\kappa^2\text{-tt})]\text{BF}_4$ (**2**) and $[(\eta^5\text{-$

Table 1 Selected interatomic distances (pm) and angles ($^\circ$) for $[(\eta^5\text{-Ind})\text{Mo}(\text{CO})_2(\kappa^2\text{-tt})]\text{BF}_4$ (**2**)

Mo–S1	254.50(6)	Mo–C11	228.2(2)
Mo–S2	257.79(5)	Mo–C12	227.7(3)
Mo–C1	196.4(2)	Mo–C13	228.1(2)
Mo–C2	196.6(2)	Mo–C13A	241.1(2)
		Mo–C17A	240.1(2)
S1–Mo–S2	67.86(2)	C4–S3–C5	101.53(11)
S1–C3–S2	104.51(12)	S1–C5–S3	116.49(13)
S2–C4–S3	115.91(11)		

$\text{Ind})\text{Mo}(\text{CO})_2(\kappa^2\text{-ttcd})]\text{BF}_4$ (**3**) (Scheme 4). Complexes **2** and **3** were also obtained in good yield from $[(\eta^5\text{-Ind})\text{Mo}(\text{CO})_2(\kappa^2\text{-dme})]\text{BF}_4$ as an intermediate (with the labile 1,2-dimethoxyethane ligand).

^1H NMR analysis of $[(\eta^5\text{-Ind})\text{Mo}(\text{CO})_2(\kappa^2\text{-tt})]\text{BF}_4$ (**2**) revealed the typical pattern of resonances of the $\eta^5\text{-Ind}$ ring, with the triplet of H^2 up-field of the doublet assigned to $\text{H}^{1/3}$.^{32,33} An X-ray diffraction study confirmed this structural assignment as depicted in Fig. 1 and Table 1 (where bond distances and angles are listed). The planar indenyl ligand shows the typical deviation towards the $\eta^3 + \eta^2$ coordination mode, with the Mo–C13A and Mo–C17A bonds slightly longer than Mo–C11, Mo–C12, and Mo–C13. The fact that no ring slippage took place is intriguing, since the free S atom is in an apparently favourable position to engage in bonding with Mo. The Mo–S3 distance is however far away from a bonding interaction (363.6 pm).

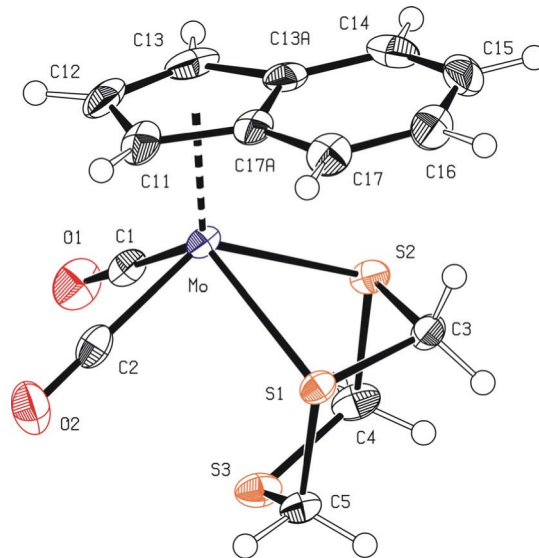


Fig. 1 ORTEP plot of the $[(\eta^5\text{-Ind})\text{Mo}(\text{CO})_2(\kappa^2\text{-tt})]^+$ cation (**2**) with the atomic numbering scheme. Thermal ellipsoids are drawn at the 50% probability level.

^1H NMR resonances of complex $[(\eta^5\text{-Ind})\text{Mo}(\text{CO})_2(\kappa^2\text{-ttcd})]\text{BF}_4$ (**3**) are also typical of $\eta^5\text{-Ind}$, leaving two coordination positions available for the ttcd ligand. We assign the ttcd–Mo bonding to two consecutive S atoms, on the basis of the ^1H NMR spectrum which presents a complex set of aliphatic resonances, due to the folding of the ligand. If coordination were established by two alternate S atoms, a simpler spectrum would result in this region, owing to the existing plane of symmetry. DFT calculations (see Computational studies below) confirm that the complex where

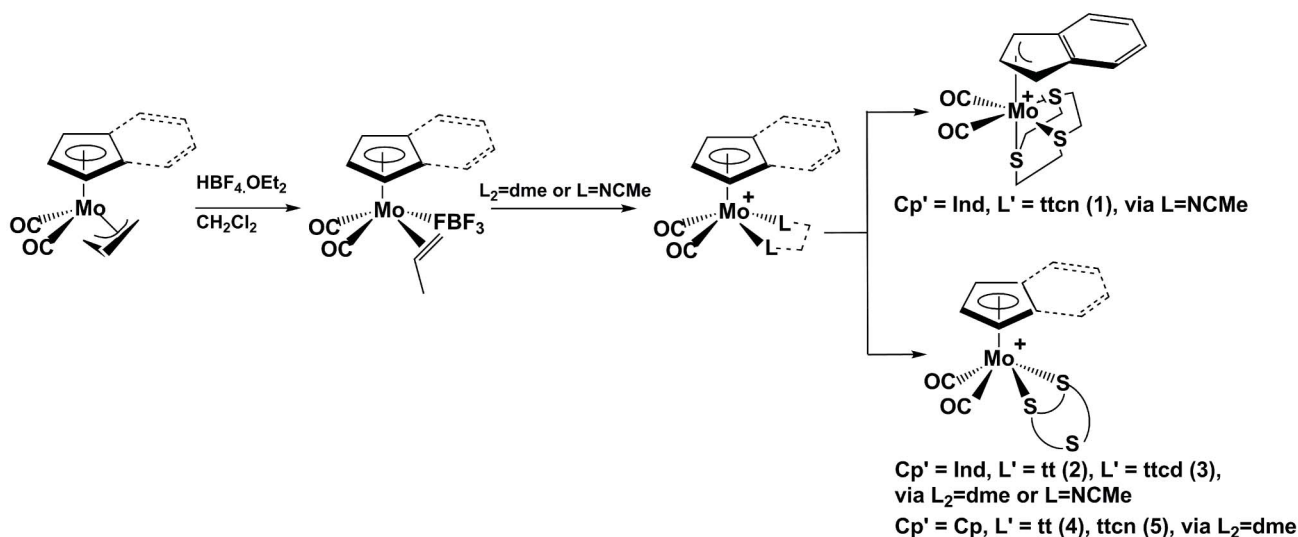


Table 2 Selected interatomic distances (pm) and angles (°) for [CpMo(CO)₂(κ²-ttcn)]BF₄ (**5**)

Mo–S1	248.34(4)	Mo–C13	229.7(2)
Mo–S2	251.33(5)	C7–C8	151.9(3)
Mo–C1	197.79(16)	C9–C10	141.1(3)
Mo–C2	197.1(2)	C9–C13	141.4(3)
Mo–C9	227.8(2)	C10–C11	141.2(3)
Mo–C10	230.5(3)	C11–C12	138.8(3)
Mo–C11	236.4(3)	C12–C13	141.1(3)
Mo–C12	236.8(2)		
S1–Mo–S2	79.41(2)	C3–S1–C8	105.06(11)
S1–Mo–C1	129.65(5)	C4–S2–C5	101.85(10)
S1–Mo–C2	79.70(6)	C6–S3–C7	103.56(11)

ttcd binds using two consecutive sulfur atoms is more stable by ~6 kcal mol⁻¹, than when it uses opposite sulfurs.

Thus, in contrast to ttcn, tt and ttcd fail to induce indenyl slippage and bind in a κ²-fashion in the respective [(η⁵-Ind)Mo(CO)₂(κ²-L)]⁺ complexes. Furthermore, complexes **2** and **3** do not undergo ring slippage upon NCMe addition. ¹H NMR spectra of NCCD₃ solutions of complexes **2** and **3** at -30 °C show loss of the macrocycles (tt or ttcd) with formation of [(η³-Ind)Mo(CO)₂(NCMe)₃]⁺.

Cyclopentadienyl congener complexes [CpMo(CO)₂(κ²-tt)]BF₄ (**4**) and [CpMo(CO)₂(κ²-ttcn)]BF₄ (**5**) were obtained from the intermediate [CpMo(CO)₂(κ²-dme)]BF₄ (Scheme 4) and no reaction occurred when [CpMo(CO)₂(NCMe)₂]⁺BF₄ was used. Complex **5** was characterised by X-ray diffraction crystallography, as depicted in Fig. 2 and Table 2. It belongs to the general family of four legged piano stool compounds, with a pentahapto Cp ring (all Mo–C bonds being similar). One S atom in ttcn ring is turned away from Mo, in a non-bonding position. This ring configuration is necessarily inverted in the complex [(η³-Ind)Mo(CO)₂(κ³-ttcn)]BF₄ (**1**).

The complex [CpMo(CO)₂(κ²-tt)]BF₄ (**4**) presents a Cp resonance in the ¹H NMR spectrum at δ 4.39 ppm. This value is shifted to high field, namely when compared to the Cp resonance of the ttcn analogue **5** (at δ 5.72 ppm). This high field shift could suggest a trihapto coordination of the Cp ring (and a [(η³-Cp)Mo(CO)₂(κ³-tt)]⁺ formulation), but this hypothesis is contradicted by the fact

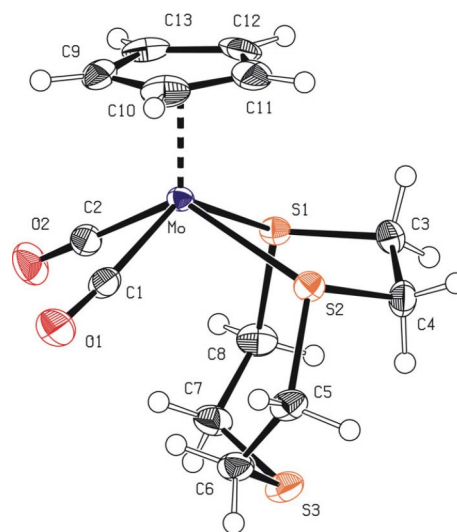


Fig. 2 ORTEP plot of the [CpMo(CO)₂(κ²-ttcn)]⁺ cation (**5**) with the atomic numbering scheme. Thermal ellipsoids are drawn at the 50% probability level.

that tt ligand failed to induce ring-slippage in the corresponding indenyl complex [(η⁵-Ind)Mo(CO)₂(κ²-tt)]BF₄ (**2**), as described above. The complex [CpMo(CO)₂(ttcd)]BF₄ could not be obtained pure.

C–S activation and 1,4,7-trithiacyclononane ring-opening reaction. Surprisingly, when ttcn reacts with IndMo(CO)₂(C₃H₆)(FBF₃) instead of [(η⁵-Ind)Mo(CO)₂-(NCMe)₂]⁺BF₄, the green complex [(η⁵-Ind)Mo(κ³-1,4,7-trithiaheptanate)(CO)]BF₄ (**6**) is rapidly formed upon ring opening of ttcn and facile dissociation of a CO ligand (Scheme 5). A small amount of **1** is also formed in the reaction.

Complex **6** has only one ν(CO) stretching vibration in the IR spectrum (at 2033 cm⁻¹) and a typical η⁵-Ind resonance pattern in the ¹H NMR spectrum. The nature of complex **6** was clarified by means of an X-ray diffraction study. Fig. 3 shows the geometry and the atom labelling scheme for the molecule and Table 3

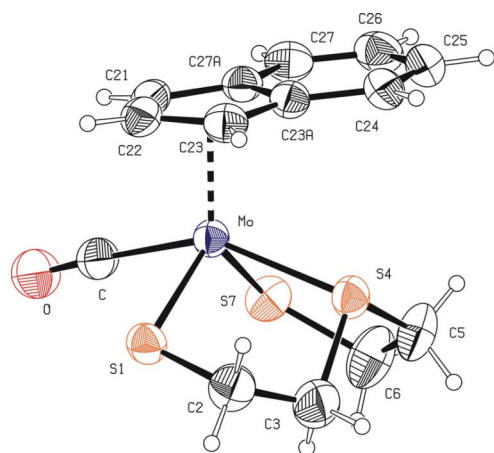
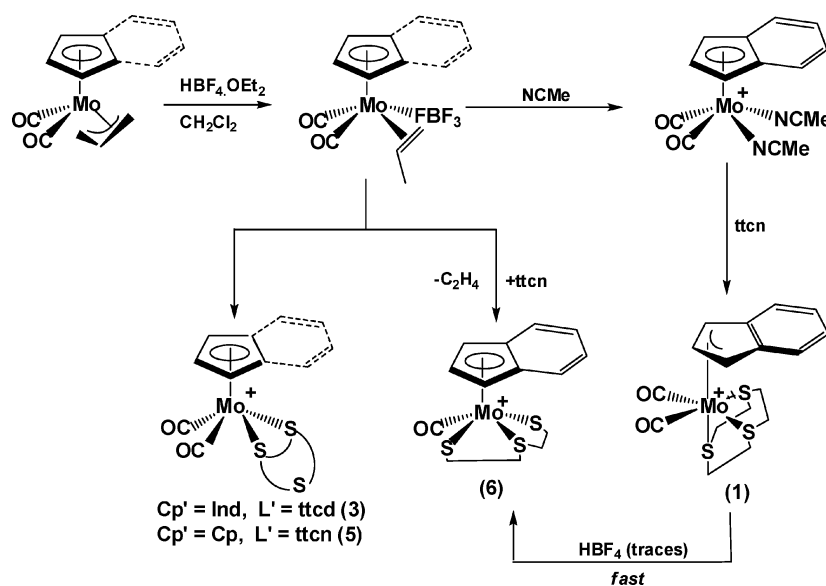


Fig. 3 ORTEP plot of $[(\eta^5\text{-Ind})\text{Mo}(\kappa^3\text{-}1,4,7\text{-trithiaheptanate})(\text{CO})]^+$ cation (**6**) with the atomic numbering scheme. Thermal ellipsoids are drawn at the 50% probability level. The BF_4^- anion is disordered in two positions.

summarises selected bond angles, distances and slip parameters. The compound is monomeric and has a formal 16 valence electron count. It belongs to the general family of four legged piano-stool compounds and bears the open tridentate tris-thiolato ligand. All intramolecular distances and angles are in the expected ranges. In general, the observed values for the ring-slippage parameters for **6** are consistent with those given in the literature^{32,40} and are typical for the $\eta^3 + \eta^2$ coordination of the indenyl ligand, with the obvious allyl-ene distortion shown by the small but definite value of $\Delta(\text{M}-\text{C})$ (15 pm). A typical alternation of shorter and longer C-C distances in the benzene part of the indenyl ligand indicates diene character (Table 3).

The unexpected formation of **6** results from the loss of an ethylene fragment from the ttcn ligand, which is accompanied by a formal two-electron oxidation of the metal from Mo(II) to Mo(IV). Such fragmentation is, however, absent in the high-yield formation of **1**. Since traces of acid can be present in the preparation of **6** as a result of the conditions of formation of

Table 3 Selected interatomic distances (pm) and angles ($^\circ$) for $[(\eta^5\text{-Ind})\text{Mo}(\kappa^3\text{-}1,4,7\text{-trithiaheptanate})(\text{CO})]\text{BF}_4$ (**6**)

Mo-S1	229.30(13)	Mo-C27A	246.4(5)
Mo-S4	247.51(12)	C2-C3	149.3(8)
Mo-S7	232.21(14)	C5-C6	139.1(10)
Mo-C	201.3(5)	C21-C22	140.9(7)
Mo-C21	232.0(5)	C22-C23	139.5(7)
Mo-C22	229.2(5)	C23-C23A	144.1(6)
Mo-C23	228.7(5)	C23A-C27A	141.8(6)
Mo-C23A	243.3(4)	C21-C27A	142.3(6)
S1-Mo-S4	83.16(4)	S4-Mo-S7	83.37(5)
S1-Mo-S7	112.84(5)	S4-Mo-C	150.01(16)
S1-Mo-C	80.77(16)	S7-Mo-C	79.82(16)

$(\eta^5\text{-Ind})\text{Mo}(\text{CO})_2(\text{C}_3\text{H}_6)(\text{FBF}_3)^{41}$ (Scheme 5), we reasoned that **6** is possibly formed from **1** under acid catalysis. A pure sample of complex **1** in dichloromethane converted slowly to **6**, in 6% conversion (or 5% conversion, in the absence of light), after 7 h at room temperature, with loss of ethylene, as confirmed by ^1H NMR. The addition of a drop of HBF_4 , on the other hand, led to a very rapid, almost immediate reaction, with full conversion of complex **1** into **6** after 10 min at room temperature, confirming the occurrence of acid catalysis.

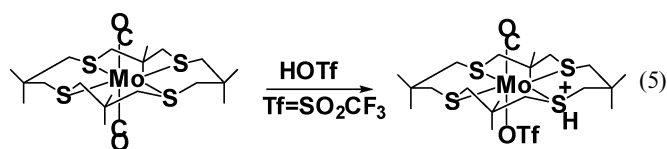
Accordingly, the reaction of the *in situ* generated intermediate $[(\eta^5\text{-Ind})\text{Mo}(\text{CO})_2(\text{dme})]^+$ with ttcn leads to the formation of complex **1** contaminated by complex **6** (5% contamination, after 2 h), owing to the presence of acid in the reaction media. On continuation of the reaction, the full conversion of **1** into **6** is observed.

Acid-catalysed reactions involving complexed sulfur macrocyclic ligands have been documented. Indeed, thioether ligands are π -acids (with an accepting strength between that of amines and phosphines) and when protonated they become even stronger π -acids, as shown by Yoshida and co-workers on their reported study of the first secondary sulfonium ion complex $\text{trans}[\text{Mo}(\text{CO})(\text{OTf})(\text{syn-Me}_8\text{H}[16]\text{janeS}_4)]^+$ prepared through S-protonation of $\text{trans}[\text{Mo}(\text{CO})_2(\text{syn-Me}_8[16]\text{janeS}_4)]$ with HOTf (eqn (1) and (5)).⁴²

Table 4 Relative energies (E_r) for $[(\eta^{3/5}\text{-Cp/Ind})\text{Mo}(\kappa^{3/2}\text{-macrocycle})(\text{CO})_2]^+$ complexes

Complex	$E_r/\text{kcal mol}^{-1}$	Complex	$E_r/\text{kcal mol}^{-1}$
$[(\eta^5\text{-Cp})\text{Mo}(\text{CO})_2(\kappa^2\text{-tt})]^+$	0	$[(\eta^3\text{-Cp})\text{Mo}(\text{CO})_2(\kappa^3\text{-tt})]^+$	33.0
$[(\eta^5\text{-Cp})\text{Mo}(\text{CO})_2(\kappa^2\text{-ttcn})]^+$	0	$[(\eta^3\text{-Cp})\text{Mo}(\text{CO})_2(\kappa^3\text{-ttcn})]^+$	22.2
$[(\eta^5\text{-Cp})\text{Mo}(\text{CO})_2(\kappa^2\text{-ttcd})]^+{}^a$	0	$[(\eta^3\text{-Cp})\text{Mo}(\text{CO})_2(\kappa^3\text{-ttcd})]^+$	16.3
$[(\eta^5\text{-Cp})\text{Mo}(\text{CO})_2(\kappa^2\text{-ttcd})]^+{}^b$	2.6		
$[(\eta^5\text{-Ind})\text{Mo}(\text{CO})_2(\kappa^2\text{-tt})]^+$	0	$[(\eta^3\text{-Ind})\text{Mo}(\text{CO})_2(\kappa^3\text{-tt})]^+$	15.4
$[(\eta^5\text{-Ind})\text{Mo}(\text{CO})_2(\kappa^2\text{-ttcn})]^+{}^c$	0	$[(\eta^3\text{-Ind})\text{Mo}(\text{CO})_2(\kappa^3\text{-ttcn})]^+{}^c$	6.4
$[(\eta^5\text{-Ind})\text{Mo}(\text{CO})_2(\kappa^2\text{-ttcd})]^+{}^a$	0	$[(\eta^3\text{-Ind})\text{Mo}(\text{CO})_2(\kappa^3\text{-ttcd})]^+$	1.24
$[(\eta^5\text{-Ind})\text{Mo}(\text{CO})_2(\kappa^2\text{-ttcd})]^+{}^b$	6.0		

^a Binding through two consecutive sulfur atoms ^b Binding through two opposite sulfur atoms. ^c Most stable indenyl conformation selected (see Fig. 5 below).



The ring-opening reaction does not take place for ttcd macrocycle, neither in indenyl nor in cyclopentadienyl systems (Scheme 5).

Computational studies: structures and preferences. There are several open questions in the previous experimental results, namely (1) the formation of the slipped η^3 -derivative in the reaction of ttcn and $[(\eta^5\text{-Ind})\text{Mo}(\text{CO})_2(\text{NCMe})_2]\text{BF}_4$, contrarily to the formation of the η^5 -indenyl complexes with the other macrocycles, tt and ttcd; (2) the preferred structure of the ttcd complex; (3) the mechanism for the loss of ethylene in the ttcn system.

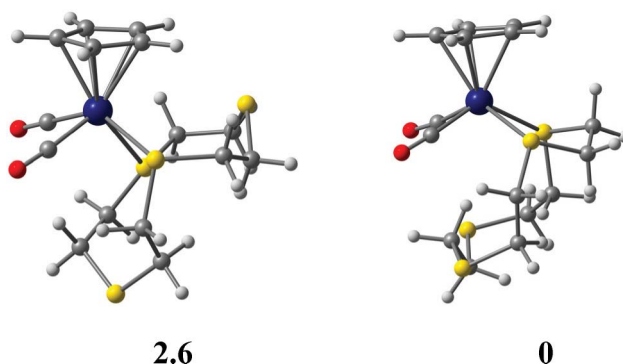
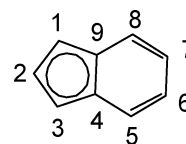
DFT calculations³⁹ (Gaussian 03,⁴³ see Computational details) were performed in models obtained from the two experimental structures described above (Fig. 1 and 2).

The lowest energy is always found for the η^5 -ring coordination (Cp, Ind, tt, ttcn or ttcd). The available X-ray structures showed that it is indeed the case for the $[(\eta^5\text{-Ind})\text{Mo}(\text{CO})_2(\kappa^2\text{-tt})]^+$ (**2**) and $[(\eta^5\text{-Cp})\text{Mo}(\text{CO})_2(\kappa^2\text{-ttcn})]^+$ (**5**) cations. NMR evidence indicates the presence of η^5 -coordination in the two ttcd complexes, both with Cp and Ind. There is only one exception, namely $[(\eta^3\text{-Ind})\text{Mo}(\text{CO})_2(\kappa^3\text{-ttcn})]^+$ was the only indenyl complex of ttcn isolated and characterised, and the η^5 -Ind isomer was never detected in solution. Before analysing this issue, there is the question of the coordination mode of ttcd. As mentioned in Table 4, in the most stable isomer the ttcd ligand binds to molybdenum using two consecutive sulfur atoms (Fig. 4). The geometries calculated for the analogous indenyl complexes are very similar.

The calculated structures reproduce very well the two determined ones, as shown by a few selected data given in Table 5, with

Table 5 Selected calculated and experimental distances (pm) in $[(\eta^5\text{-Cp})\text{Mo}(\text{CO})_2(\kappa^2\text{-ttcn})]^+$ and $[(\eta^5\text{-Ind})\text{Mo}(\text{CO})_2(\kappa^2\text{-tt})]^+$

	$[(\eta^5\text{-Cp})\text{Mo}(\text{CO})_2(\kappa^2\text{-ttcn})]^+$		$[(\eta^5\text{-Ind})\text{Mo}(\text{CO})_2(\kappa^2\text{-tt})]^+$	
	Exp.	Calc.	Exp.	Calc.
Mo-C2	227.8	226.6	227.7	225.4
Mo-C1,3	230.5, 229.7	230.7, 230.9	228.2, 228.1	229.7, 229.8
Mo-C4,9	236.8, 236.4	240.8, 240.8	240.1, 241.1	239.4, 239.6
Mo-S1,2	248.3, 251.3	251.9, 253.8	254.5, 257.8	256.5, 256.8
Mo-S3 (axial)	460.6	464.4	363.6	367.4

**Fig. 4** Optimised geometries of the $[(\eta^5\text{-Cp})\text{Mo}(\kappa^2\text{-1,4,7,10-ttcd})(\text{CO})_2]^+$ cation with different ligand coordination with relative energies (kcal mol^{-1}).

the distances typical of the $\eta^3 + \eta^2$ coordination in the indenyl complex and closer Mo-C distances with Cp.

In the η^5 -Ind complexes, the benzene substituent lies over the macrocycle, being *trans* to the carbonyls. This is the orientation experimentally found for $[(\eta^5\text{-Ind})\text{Mo}(\text{CO})_2(\kappa^2\text{-tt})]^+$, and was found to be also the most stable in the ttcn complex, where the three more important conformations were studied (Fig. 5). In this case, the conformer with the indenyl rotated $\sim 90^\circ$ has an energy 5.1 kcal mol^{-1} higher and the one with 180° rotation (benzene over the carbonyls) 9.0 higher. The differences are small.

The preferences are much more defined in the η^3 -Cp complexes. Slippage and bending only occur when the two non-bonded carbon atoms are on the side of the carbonyls (Fig. 6, a). No η^3 -Cp structures could be successfully obtained from optimising geometries with other arrangements. For the indenyl derivatives, a more complete study with the ttcn ligand showed small energy differences for the three conformers analysed, as shown in Fig. 6. The lowest energy η^3 -Ind species (**d**) has the indenyl with the

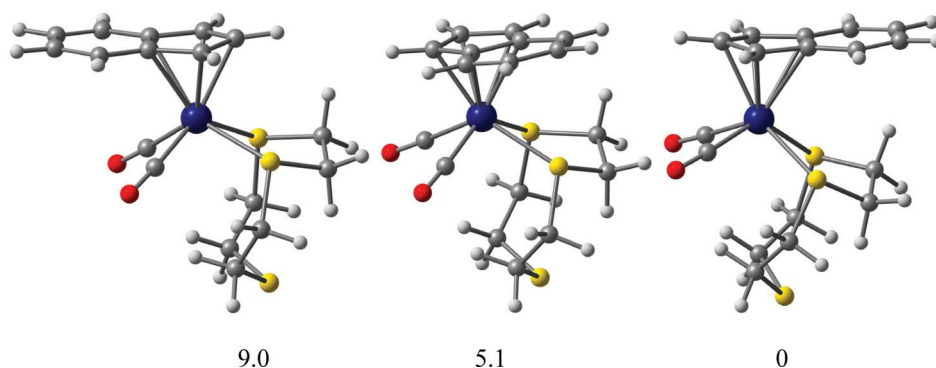


Fig. 5 Optimised geometries of the $[(\eta^5\text{-Ind})\text{Mo}(\kappa^2\text{-1,4,7-ttcn})(\text{CO})_2]^+$ cation with different indenyl arrangements and relative energies (kcal mol^{-1}).

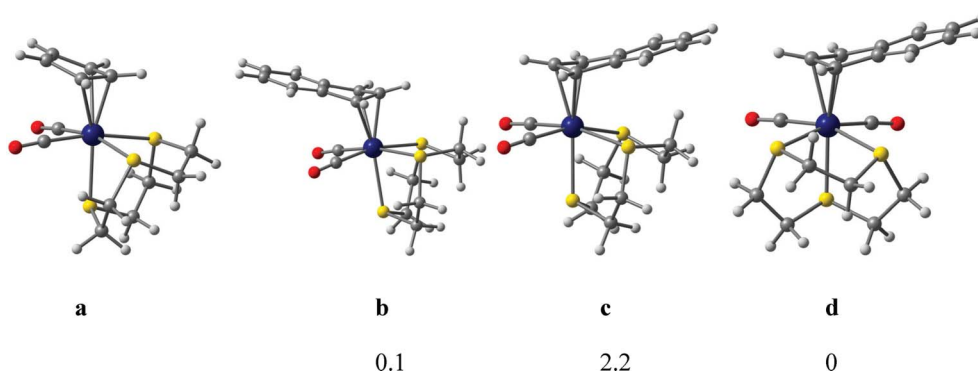


Fig. 6 Optimised geometries of $[(\eta^3\text{-Cp})\text{Mo}(\kappa^3\text{-1,4,7-ttcn})(\text{CO})_2]^+$ (**a**), and the $[(\eta^3\text{-Ind})\text{Mo}(\kappa^3\text{-1,4,7-ttcn})(\text{CO})_2]^+$ cation with three different indenyl arrangements (**b–d**) and relative energies (kcal mol^{-1}).

benzene between one CO and one sulfur of the macrocycle, but the differences are small.

The arrangement **c** was preferred for the ttcn derivative ($6.5 \text{ kcal mol}^{-1}$), while for tt the energy difference was negligible.

A further look at the values in Table 4 shows that the $\eta^3\text{-Ind}$ complex $[(\eta^3\text{-Ind})\text{Mo}(\kappa^3\text{-1,4,7-ttcn})(\text{CO})_2]^+$ is not particularly more stable than others, relative to the $\eta^5\text{-Ind}$, from the thermodynamic point of view. Therefore, we looked for the factors that might favour the formation of this slipped isomer when ttcn is present, and make it a kinetic isomer. The macrocycles may exist in different conformations, differing in the dihedral angles, and resulting in different arrangements of the sulfur atoms and energies. Drew and co-workers confirmed this for ttcn using several conformational search methods, including high-temperature molecular dynamics in vacuum and with the universal force field.⁴⁴ The authors identified several distinct conformations using, as separation criteria, the molecular mechanics energies together with RMSD (root mean square deviation). Unfortunately, many of the obtained conformers share similar SCCS torsion angle profiles and their overall observation frequencies might not be a good estimation of this macrocycle conformational preferences in solution.

The conformational spaces of the macrocycles were thus studied using molecular dynamics (MD, see Computational details), and structures were grouped according to their conformational clusters. For the small tt macrocycle, there are two main structures, chair and boat, with ~ 67 and $\sim 33\%$ of all conformations, respectively. The minimum energy geometries were obtained from the MD's cluster minima and optimised with DFT, showing that the energy of the chair conformation is $\sim 3 \text{ kcal mol}^{-1}$ lower than

the boat one. The chair conformation has been experimentally found in the $\kappa^2\text{-tt}$ coordination of $[(\eta^5\text{-Ind})\text{Mo}(\text{CO})_2(\kappa^2\text{-tt})]^+$ (Fig. 1) and is also the one required in $\kappa^3\text{-tt}$ coordination of $[(\eta^3\text{-Ind})\text{Mo}(\text{CO})_2(\kappa^3\text{-tt})]^+$ (as confirmed by DFT calculations).

The ttcn conformers fall into two main clusters: (1) all three SCCS dihedral angles are $\pm 60^\circ$ and the three sulfur atoms face the same side; (2) only two SCCS dihedral angles are $\pm 60^\circ$, and one sulfur is pointing away from the others. The first cluster covers 99.7% of all conformations. The minimum DFT energy structure is found in the first group, while in the second a conformer with $0.3 \text{ kcal mol}^{-1}$ higher energy is obtained. This indicates that almost all the molecules in solution have the three sulfur atoms pointing in the same direction (Fig. 7). For the $\eta^5\text{-Ind/Cp}$ coordination (see Fig. 2), the $\kappa^2\text{-ttcn}$ ligand requires conformations from the second cluster (with two sulfurs on one side, one sulfur on the other), which are practically unavailable in solution. They would have to rearrange. On the other hand, the vast majority of molecules have the appropriate conformation (first cluster) for $\kappa^3\text{-ttcn}$ coordination, which is associated with $\eta^3\text{-Ind}$. These observations support the idea that the observed complex is the kinetically favoured species and not the thermodynamic one and are sketched in Scheme 6.

Upon replacement of the first NCMe ligand by an incoming S atom of the ttcn ring, one NCMe would remain in the metal coordination sphere, and a species like **e** or **e'** becomes a likely intermediate (Scheme 6). Loss of the second MeCN from **e'** would lead to $[(\eta^5\text{-Ind})\text{Mo}(\kappa^2\text{-1,4,7-ttcn})(\text{CO})_2]^+$. However, the ttcn molecules in solution have the other conformation, so that **e** is more likely to be formed, leading to the intermediate **f**, where

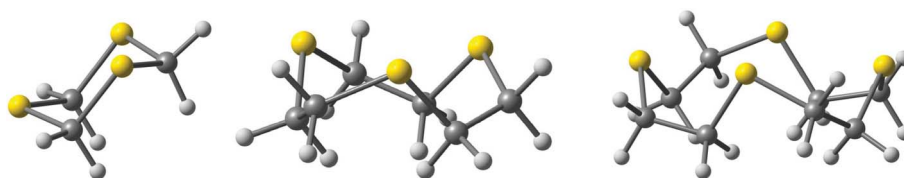
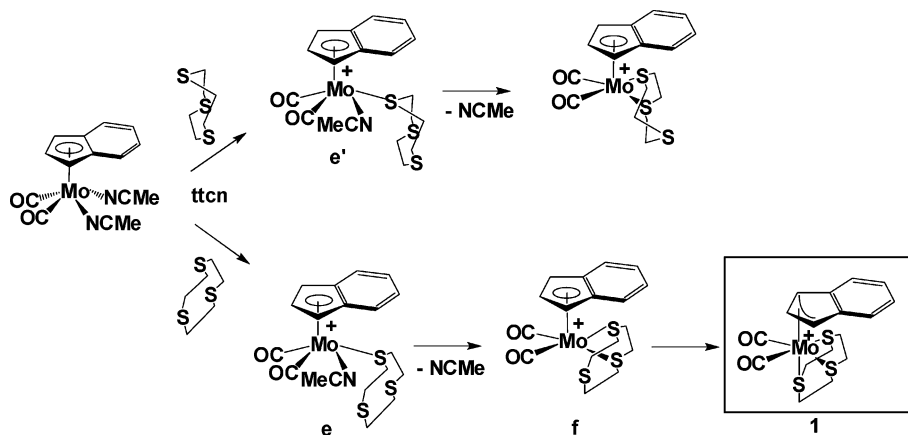
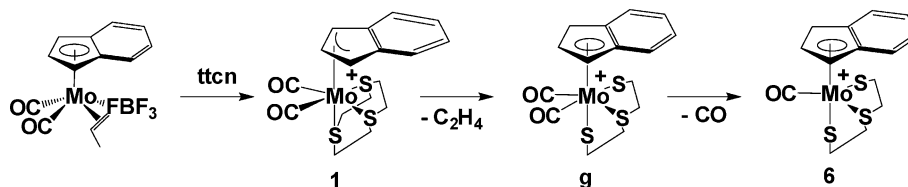


Fig. 7 Optimised geometries of the major conformers of tt (left), ttcn (center) and ttcd (right).



Scheme 6



Scheme 7

the distance from Mo to the third sulfur is small and ring slippage with coordination of κ^3 -ttcn occurs, with a small barrier (9.8 kcal mol⁻¹). It is noted that the energy difference between η^5 and η^3 derivatives is only 6.4 kcal mol⁻¹; in the Cp derivatives, the energy difference between analogous isomers rises up to 22.2 kcal mol⁻¹ (Table 4) and Cp does not undergo ring slippage so easily as Ind.¹⁵

The third macrocycle (ttcd), owing to its size and flexibility, generated a larger amount of conformational clusters from the MD studies. We observed five main clusters with the major one representing a population of 48.1%. It is characterised by a very regular structure with all SCCS dihedral angles around $\pm 60^\circ$, and all S atoms facing the same side (Fig. 7, c). This is the typical crown-ether structure, with four sulfur atoms approximately in one plane. There are three other clusters with an increasing number of sulfurs deviating from that plane, namely one (30.3%), two (4.1%) or three (12.3%) S atoms. In the fifth cluster (5.2%) two S atoms are facing the opposite sides of that plane. It should be mentioned that, whenever two S atom distortions are obtained, these atoms are always side-by-side. An analysis from our clusters regarding the availability of side-by-side *vs.* cross S atoms revealed that the sequential distribution of S atoms is preferred (70%). In this macrocycle there is, thus, a complete agreement between the ligand conformational space accessed with MD, the molybdenum complex optimization energies from DFT calculations (Fig. 4), and the NMR experimental evidences.

Computational studies: C–S activation and 1,4,7-trithiacyclononane ring opening reaction.

As described above (Scheme 5) the attempts at synthesizing the macrocycle complex directly from IndMo(CO)₂(C₃H₆)(FBF₃) and ttcn, without isolating $[(\eta^5\text{-Ind})\text{Mo}(\text{CO})_2(\text{NCMe})_2]\text{BF}_4$, did not afford complex **1**, as expected, but another complex resulting from loss of ethylene and loss of CO (**6**, Scheme 7). The reaction between IndMo(CO)₂(C₃H₆)(FBF₃) and another macrocycle, ttcd, however, gave the $[(\eta^5\text{-Ind/Cp})\text{Mo}(\text{CO})_2(\kappa^2\text{-ttcd})]^+$ complex, exactly as when $[(\eta^5\text{-Ind})\text{Mo}(\text{CO})_2(\text{NCMe})_2]\text{BF}_4$ was isolated (Scheme 5). Several experimental observations showed that pure **1** in dichloromethane solution slowly transformed into **6**. In the presence of a small amount of acid, the reaction was catalysed and went to completion in a shorter time.

Ethylene loss from complexed ttcn was described by Blower and co-workers, who have shown that the reduction of the thioether complex $[\text{Re}(\text{ttcn})_2]^{2+}$ leads to ethylene loss with formation of $[\text{Re}(\text{ttcn})(\text{SCH}_2\text{CH}_2\text{SCH}_2\text{CH}_2\text{S})]^+$ (eqn (3), Scheme 3). This cleavage supports the notion that C–S σ^* orbitals accept electron density from metal-based orbitals, leading to lengthening of C–S bond and, in extreme cases, to complete cleavage under mild conditions, to release ethylene.³⁴ This system was addressed using Car–Parrinello molecular dynamics and DFT.⁴⁵

The energy profile for the reaction calculated with DFT is shown in Fig. 8. The conformation of η^3 -Ind in

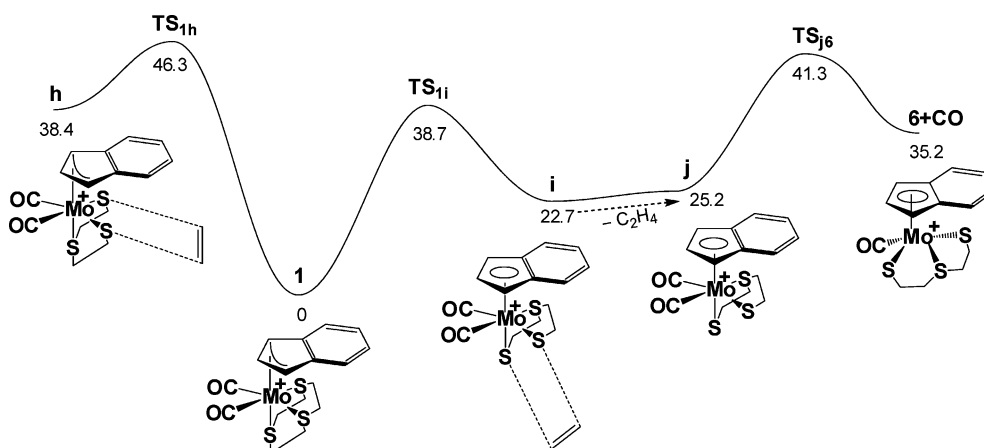


Fig. 8 Energy profile for loss of ethylene from $[(\eta^3\text{-Ind})\text{Mo}(\kappa^3\text{-1,4,7-ttcn})(\text{CO})_2]^+$, followed by loss of CO (electronic energies, kcal mol⁻¹).

$[(\eta^3\text{-Ind})\text{Mo}(\kappa^3\text{-1,4,7-ttcn})(\text{CO})_2]^+$ used as starting reagent has the benzene ring lying over the macrocycle (c in Fig. 6). There are two non-equivalent CH₂CH₂ groups that can be lost, one in the equatorial plane of the pseudo-octahedral complex, as shown on the left side of Fig. 8, and another one perpendicular (two equivalent groups), depicted on the right side. The activation barrier in this path is lower (38.7 kcal mol⁻¹) than in the previous one (46.3 kcal mol⁻¹). In the transition states, the distance between the sulfur atoms and the ethylene carbons is intermediate between the S–C distance in **1** and **h** or **i**. The reaction is expected to proceed from the intermediate **j**, with loss of CO. Some relevant distances in **h** and **i** are shown in Fig. 9.

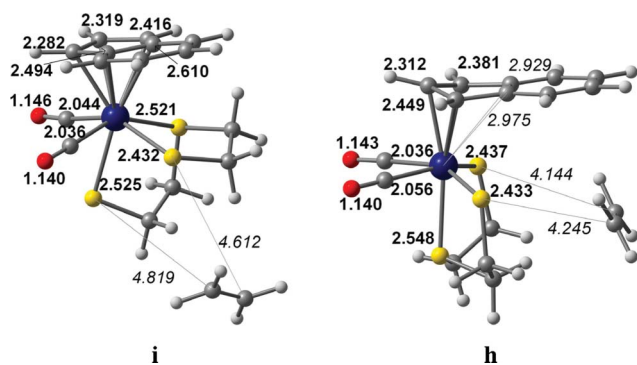


Fig. 9 Optimised geometries and selected distances (Å) of intermediates obtained from $[(\eta^3\text{-Ind})\text{Mo}(\kappa^3\text{-1,4,7-ttcn})(\text{CO})_2]^+$, after ethylene has become weakly bound.

One interesting aspect of these van der Waals complexes between species **j** and ethylene, is that the lowest energy one (**i**) can be considered a $\eta^5\text{-Ind}$ complex, with five Mo–C distances ranging from 228.2 and 261.0 pm, the last one being the only one which is excessively long. The indenyl has also rotated and the complex can be formally considered an 18-electron Mo(IV) species. On the other hand, intermediate **h** has a $\eta^3\text{-Ind}$ ligand and is electronically unsaturated. As observed experimentally, loss of CO leads to the 16-electron Mo(IV) complex **6**. The high formal oxidation state leads to weak Mo–C(O) bonds, as reflected in the long calculated distances of 203.6 and 204.4 pm (**i**). In **1**, these distances are 196.6 and 199.3 pm, respectively. It is therefore not surprising that the loss of CO takes place. The reaction is helped

by the formation of gaseous products (ethylene and CO), which are liberated from the solution. The highest barrier calculated corresponds to ethylene loss (38.7 kcal mol⁻¹) and is consistent with the slow process taking place when complex **1** is dissolved until **6** is formed. The acid-catalysed reaction has not been well enough characterised for meaningful calculations to be performed.

Conclusions

The synthetic, structural and computational studies described allow for a close comparison of the structural modifications undergone in a family of organometallic molybdenum complexes bearing two rather different types of structurally flexible ligands: the cyclopentadienyl or indenyl rings and the macrocyclic polythiaalkanes. The coordination of this type of thioether ligands is strongly influenced by their conformation and the tendency to favour chelation. Whereas the macrocycles *tt* and *ttd* present several accessible conformers and high flexibility, and coordinate the $[(\eta^3\text{-Ind})\text{Mo}(\text{CO})_2]$ fragment in a bidentate fashion to give the $[(\eta^3\text{-Ind})\text{Mo}(\text{CO})_2(\kappa^2\text{-S}_2)]^+$ species (S₂ = two ring S atoms bound), the *ttcn* ligand was able to add its third S atom and force a haptotropic shift of the indenyl ring, to form $[(\eta^3\text{-Ind})\text{Mo}(\text{CO})_2(\kappa^3\text{-ttcn})]^+$. This fact is driven by the almost exclusive presence of a single conformer of the *ttcn* ligand in solution. This conformer, with all three S atoms on the same face, presents the ideal geometry to achieve the indenyl ring slippage, which would otherwise be a thermodynamically unfavourable process. The pathway to ethylene and CO extrusion from this complex was identified, but the origin of its H⁺-catalysed activation could not yet be identified. The importance of these conformational changes in organometallic complexes bearing classical ligands, often with biological significance, is an important point to have in mind when attempting to rationalise reactivity in bio-organometallic contexts.

Experimental

All experiments were carried out under dry nitrogen using Schlenk techniques. Solvents were dried by standard procedures (diethyl ether over Na/benzophenone ketyl; dichloromethane and acetonitrile with CaH₂), distilled under argon and kept over 4 Å molecular sieves (3 Å for NCMe). Microanalyses were performed

in our laboratories (ITQB). ^1H NMR spectra were obtained with a Bruker AMX 300 MHz spectrometer and Bruker Avance II 400 MHz spectrometer. Infrared spectra were recorded in a Unicam Mattson Mod 7000 FTIR spectrophotometer using KBr pellets.

$\text{IndMo}(\text{CO})_2(\eta^3\text{-C}_3\text{H}_5)$, $\text{CpMo}(\text{CO})_2(\eta^3\text{-C}_3\text{H}_5)$, $[\text{IndMo}(\text{CO})_2\text{-}(\text{NCMe})_2]\text{BF}_4$ and $[\text{CpMo}(\text{CO})_2(\text{NCMe})_2]\text{BF}_4$ were prepared as reported.^{41b,c} 1,4,7-trithiacyclononane, 1,3,5-trithiane and 1,4,7,10-tetrathiacyclododecane were obtained commercially.

Preparation of $[(\eta^5\text{-Ind})\text{Mo}(\text{CO})_2(\kappa^2\text{-tt})]\text{BF}_4$ (2)

Method a. A solution of $(\eta^5\text{-Ind})\text{Mo}(\text{CO})_2(\eta^3\text{-C}_3\text{H}_5)$ (0.30 g, 0.97 mmol) in CH_2Cl_2 was treated with $\text{HBF}_4\cdot\text{Et}_2\text{O}$ (1 eq.). After 10 min, dme was added in excess and the reaction was left for 15 min. 1,3,5-trithiane (0.166 g, 1.2 mmol) was added and the reaction was left for 2 h at r.t. After concentration and addition of diethyl ether, an orange powder precipitated.

Method b. 1,3,5-Trithiane (0.04 g, 0.29 mmol) was added to a solution of $[\text{IndMo}(\text{CO})_2(\text{NCMe})_2]\text{BF}_4$ (0.10 g, 0.23 mmol) in CH_2Cl_2 and the reaction was left for 3 h at r.t. After concentration and addition of diethyl ether, an orange powder precipitated. The product was recrystallised from $\text{CH}_2\text{Cl}_2\text{-Et}_2\text{O}$. Yield: 98%. Crystals suitable for X-ray analysis were obtained after slow precipitation at +4 °C. Anal. Found: C, 33.79; S, 19.44; H, 2.19. Calc. for $\text{C}_{14}\text{H}_{13}\text{BF}_4\text{O}_2\text{S}_3\text{Mo}$: C, 34.17; S, 19.54; H, 2.64%. Selected IR (KBr, cm^{-1}): 1992, 1901, vs, $\nu(\text{CO})$. ^1H NMR (CD_2Cl_2 , r.t., δ (ppm)): 7.84 (m, 2H, H^{5-8}), 7.70 (m, 2H, H^{5-8}), 6.15 (d, 2H, $\text{H}^{1/3}$), 5.22 (t, 1H, H^2), 4.83 (c, 2H, H^{tt}), 4.14 (br, 4H, H^{tt}). ^{13}C NMR (CD_2Cl_2 , r.t., δ (ppm)): 243.81 (CO), 130.91 ($\text{C}^{5/8}$), 127.52 ($\text{C}^{6/7}$), 115.60 ($\text{C}^{4/9}$), 90.23 (C^2), 79.29 ($\text{C}^{1/3}$), 35.82 (tt).

Preparation of $[(\eta^5\text{-Ind})\text{Mo}(\text{CO})_2(\kappa^2\text{-ttcd})]\text{BF}_4$ (3)

Method a. Same procedure as for complex 2 (see above), with $\text{IndMo}(\text{CO})_2(\eta^3\text{-C}_3\text{H}_5)$ (0.15 g, 0.48 mmol), $\text{HBF}_4\cdot\text{Et}_2\text{O}$ (1 eq.), excess dme and 1,4,7,10-tetrathiacyclododecane (0.12 g, 0.5 mmol).

Method b. Same procedure as for complex 2 (see above), with $[\text{IndMo}(\text{CO})_2(\text{NCMe})_2]\text{BF}_4$ (0.10 g, 0.23 mmol) and 1,4,7,10-tetrathiacyclododecane (0.066 g, 0.27 mmol). The orange product was recrystallised from $\text{CH}_2\text{Cl}_2\text{-Et}_2\text{O}$. Yield: 90%. Selected IR (KBr, cm^{-1}): 1961, 1889, vs, $\nu(\text{CO})$. ^1H NMR (CD_2Cl_2 , r.t., δ (ppm)): 7.64 (m, 2H, H^{5-8}), 7.54 (m, 2H, H^{5-8}), 6.29 (d, 2H, $\text{H}^{1/3}$), 5.32 (t, 1H, H^2), 3.48–2.67 (c, 16H, H^{ttcd}). ^{13}C NMR (CD_2Cl_2 , r.t., δ (ppm)): 243.27 (CO), 131.16 ($\text{C}^{5/8}$), 127.47 ($\text{C}^{6/7}$), 117.80 ($\text{C}^{4/9}$), 88.89 (C^2), 79.12 ($\text{C}^{1/3}$), 38.65, 34.56, 32.28, 31.68, 28.96 (ttcd). ESI/positive mode: m/z 506.9 (M^+ , $[\text{IndMo}(\text{CO})_2(\text{ttcd})]^+$).

Preparation of $[\text{CpMo}(\text{CO})_2(\kappa^2\text{-tt})]\text{BF}_4$ (4)

A solution of $\text{CpMo}(\text{CO})_2(\eta^3\text{-C}_3\text{H}_5)$ (0.250 g, 0.97 mmol) in CH_2Cl_2 was treated with $\text{HBF}_4\cdot\text{Et}_2\text{O}$ (1 eq.). After 10 min dme was added in excess and the reaction was left for 15 min. 1,3,5-Trithiane (0.13 g, 0.97 mmol) was added and the reaction was left for 2 h at r.t.. After concentration and addition of diethyl ether, an orange complex precipitated. This was recrystallised from $\text{CH}_2\text{Cl}_2\text{-Et}_2\text{O}$. Yield: 90%. Anal. Found: C, 27.2; S, 21.8; H, 2.39. Calc. for $\text{C}_{10}\text{H}_{11}\text{BF}_4\text{O}_2\text{S}_3\text{Mo}$: C, 27.2; S, 21.7; H, 2.51%. Selected

IR (KBr, cm^{-1}): 1967, 1893, vs, $\nu(\text{CO})$. ^1H NMR ($(\text{CD}_3)_2\text{CO}$, r.t., δ (ppm)): 4.39 (s, 5H, Cp), 3.71 (br, 2H, H^{tt}), 2.53 (br, 4H, H^{tt}).

Preparation of $[\text{CpMo}(\text{CO})_2(\kappa^2\text{-ttcn})]\text{BF}_4$ (5)

Method a. A solution of $\text{CpMo}(\text{CO})_2(\eta^3\text{-C}_3\text{H}_5)$ (0.347 g, 1.35 mmol) in CH_2Cl_2 was treated with $\text{HBF}_4\cdot\text{Et}_2\text{O}$ (1 eq.). After 10 min, dme was added in excess and the reaction was left for 15 min. 1,4,7-Trithiacyclononane (0.24 g, 1.35 mmol) was added and the reaction was left for 2 h at r.t.. After concentration and addition of diethyl ether, the orange complex precipitated.

Method b. A solution of $\text{CpMo}(\text{CO})_2(\eta^3\text{-C}_3\text{H}_5)$ (0.065 g, 0.25 mmol) in CH_2Cl_2 was treated with $\text{HBF}_4\cdot\text{Et}_2\text{O}$ (1 eq.). After 10 min, 1,4,7-trithiacyclononane (0.045 g, 0.25 mmol) was added and the reaction left for 2 h at r.t.. After concentration and addition of diethyl ether, the orange complex precipitated. This was recrystallised from $\text{CH}_2\text{Cl}_2\text{-Et}_2\text{O}$. Crystals suitable for X-ray analysis were obtained after slow precipitation at +4 °C. Yield: 90%. Anal. Found: C, 32.02; S, 19.46; H, 3.51. Calc. for $\text{C}_{13}\text{H}_{17}\text{BF}_4\text{O}_2\text{S}_3\text{Mo}$: C, 32.25; S, 19.86; H, 3.54%. Selected IR (KBr, cm^{-1}): 1967, 1893, vs, $\nu(\text{CO})$. ^1H NMR (CD_2Cl_2 , r.t., δ (ppm)): 5.72 (s, 5H, Cp), 3.88–2.45 (c, 12H, H^{ttcn}). ^{13}C NMR (CD_2Cl_2 , r.t., δ (ppm)): 243.76 (CO), 96.33 (Cp), 42.43, 41.31, 37.31 (ttcn).

Preparation of $[(\eta^5\text{-Ind})\text{Mo}(\kappa^3\text{-1,4,7-trithiaheptanate})(\text{CO})]\text{BF}_4$ (6)

A solution of $\text{IndMo}(\text{CO})_2(\eta^3\text{-C}_3\text{H}_5)$ (0.20 g, 0.65 mmol) in CH_2Cl_2 was treated with $\text{HBF}_4\cdot\text{Et}_2\text{O}$ (1 eq.). After 10 min, 1,4,7-trithiacyclononane (0.12 g, 0.65 mmol) was added and the reaction left for 2 h at r.t.. After concentration and addition of diethyl ether, a green crystalline product precipitated simultaneously with a very small amount of complex 1. The green crystalline product was separated by a slow $\text{CH}_2\text{Cl}_2\text{-Et}_2\text{O}$ recrystallization. Yield: 70%. Anal. Found: C, 35.00; H, 3.19. Calc. for $\text{C}_{14}\text{H}_{17}\text{BF}_4\text{O}_3\text{S}_3\text{Mo}$: C, 35.02; H, 3.57%. Selected IR (KBr, cm^{-1}): 2033, vs, $\nu(\text{CO})$. ^1H NMR (NCCD_3 , r.t., δ (ppm)): 7.54–7.44 (m, 4H, H^{5-8}), 6.40 (d, 2H, $\text{H}^{1/3}$), 5.25 (t, 1H, H^2), 3.46–3.40 (m, CH_2 , H^{ttcn}), 3.25–3.10 (m, CH_2 , H^{ttcn}); 3.05–2.96 (m, CH_2 ; H^{ttcn}). ^{13}C NMR (CD_2Cl_2 , r.t., δ (ppm)): 214.81 (CO), 132.94 ($\text{C}^{5/8}$), 126.75 ($\text{C}^{6/7}$), 116.38 ($\text{C}^{4/9}$), 88.28 (C^2), 87.22 ($\text{C}^{1/3}$), 43.67, 38.42 (trithiaheptanate).

Crystallography. Single-crystal X-ray structure determination of compounds 2, 5 and 6

Compound 2. Crystal data and details of the structure determination are presented in Table 6. Suitable single crystals for the X-ray diffraction study were grown from dichloromethane/diethyl ether/water (1:1:traces). A clear orange fragment was stored under perfluorinated ether, transferred in a Lindemann capillary, fixed and sealed. Preliminary examination and data collection were carried out on an area detecting system (NONIUS, MACH3, κ -CCD) at the window of a rotating anode (NONIUS, FR951) and graphite monochromated Mo-K α radiation ($\lambda = 0.71073$ Å). The unit cell parameters were obtained by full-matrix least-squares refinement of 3174 reflections. Data collection were performed at 173 K (OXFORD CRYOSYSTEMS) within a θ -range of $2.11 < \theta < 25.36^\circ$. Nine data sets were measured in rotation scan mode with $\Delta\phi/\Delta\Omega = 2.0^\circ$. A total number of 17320 intensities were

Table 6 Summary of the crystal data and details of data collection and refinement for compounds **2**, **5** and **6**

	2	5	6
Empirical formula	C ₁₄ H ₁₃ BF ₄ MoO ₂ S ₃ ·0.185H ₂ O	C ₁₃ H ₁₇ BF ₄ MoO ₂ S ₃	C ₁₄ H ₁₅ BF ₄ MoOS ₃
<i>M_r</i>	495.54	484.23	478.22
Color/habit	Orange/fragment	Orange/fragment	Dark green/prism
Crystal dimensions/mm ³	0.05 × 0.13 × 0.33	0.38 × 0.38 × 0.56	0.23 × 0.23 × 0.41
Crystal system	Triclinic	Monoclinic	Monoclinic
Space group	<i>P</i> $\bar{1}$ (no. 2)	<i>P</i> 2 ₁ / <i>c</i> (no. 14)	<i>P</i> 2 ₁ / <i>n</i> (no. 14)
<i>a</i> /Å	7.5840(1)	8.0141(1)	9.542(2)
<i>b</i> /Å	9.8657(2)	8.5400(1)	17.268(2)
<i>c</i> /Å	12.4253(2)	25.5652(3)	10.837(2)
α /°	96.8789(8)	90	90
β /°	102.5955(7)	96.1375(3)	94.07(1)
γ /°	98.2379(8)	90	90
<i>V</i> /Å ³	886.90(3)	1739.66(4)	1781.1(5)
<i>Z</i>	2	4	4
<i>D_c</i> /g cm ⁻³	1.856	1.849	1.783
μ /mm ⁻¹	1.139	1.157	1.125
<i>T</i> /K	173	173	293
<i>F</i> (000)	492	968	952
θ -range/°	2.11/25.36	2.52/25.36	2.22/24.76
Index ranges, <i>hkl</i>	±9, ±11, ±14	±9, ±10, ±30	±11, ±20, ±12
Reflections collected	17320	27903	12002
Independent reflections [<i>I</i> _o > 2σ(<i>I</i> _o)/all data/ <i>R</i> _{int}]	2937/3221/0.032	3008/3183/0.024	2528/2984/0.029
Data/restraints/parameters	3221/0/283	3183/0/285	2984/0/244
<i>R</i> ₁ ^a [<i>I</i> _o > 2σ(<i>I</i> _o)/all data]	0.0202/0.0242	0.0192/0.0210	0.0401/0.0489
<i>wR</i> ₂ ^a [<i>I</i> _o > 2σ(<i>I</i> _o)/all data]	0.0414/0.0429	0.0448/0.0456	0.1093/0.1141
GOF ^a	1.064	1.036	1.078
Weights <i>a/b</i>	0.0033/0.7138	0.0170/1.8164	0.0713/0.9586
$\Delta\rho_{\max/\min}$ /e Å ⁻³	0.48/−0.36	0.56/−0.43	0.56/−0.34

$$^a R_1 = \sum(|F_o| - |F_c|) / \sum |F_o|; wR_2 = \{ \sum [w(F_o^2 - F_c^2)^2] / \sum [w(F_o^2)^2] \}^{1/2}; GOF = \{ \sum [w(F_o^2 - F_c^2)^2] / (n - p) \}^{1/2}.$$

integrated. Raw data were corrected for Lorentz, polarization, and, arising from the scaling procedure, for latent decay and absorption effects. After merging (*R*_{int} = 0.032) a sum of 3221 (all data) and 2937 [*I* > 2σ(*I*)], respectively, remained and all data were used. The structure was solved by a combination of direct methods and difference Fourier syntheses. All non-hydrogen atoms were refined with anisotropic displacement parameters. All hydrogen atom positions were found in the difference map calculated from the model containing all non-hydrogen atoms. The hydrogen positions were refined with individual isotropic displacement parameters. The hydrogen atoms bound to the partially occupied crystal water were calculated in ideal positions of anticipated hydrogen bonds. Full-matrix least-squares refinements with 283 parameters were carried out by minimizing $\sum w(F_o^2 - F_c^2)^2$ with SHELXL-97 weighting scheme and stopped at shift/err < 0.001. The final residual electron density maps showed no remarkable features. Neutral atom scattering factors for all atoms and anomalous dispersion corrections for the non-hydrogen atoms were taken from International Tables for Crystallography.^{46d} All calculations were performed on an Intel Pentium II PC, with the STRUX-V system, including the programs PLATON, SIR92 and SHELXL-97.⁴⁶

Compound 5. Crystal data and details of the structure determination are presented in Table 6. Suitable single crystals for the X-ray diffraction study were grown from dichloromethane–diethyl ether (1:1). A clear orange fragment was stored under perfluorinated ether, transferred in a Lindemann capillary, fixed and sealed. Preliminary examination and data collection were carried out on an area detecting system (NONIUS, MACH3,

κ-CCD) at the window of a rotating anode (NONIUS, FR951) and graphite monochromated Mo-Kα radiation (λ = 0.71073 Å). The unit cell parameters were obtained by full-matrix least-squares refinement of 3414 reflections. Data collection were performed at 173 K (OXFORD CRYOSYSTEMS) within a θ -range of 2.52 < θ < 25.36°. Nine data sets were measured in rotation scan mode with $\Delta\phi/\Delta\Omega = 1.0^\circ$. A total number of 27903 intensities were integrated. Raw data were corrected for Lorentz, polarization, and, arising from the scaling procedure, for latent decay and absorption effects. After merging (*R*_{int} = 0.024) a sum of 3183 (all data) and 3008 [*I* > 2σ(*I*)], respectively, remained and all data were used. The structure was solved by a combination of direct methods and difference Fourier syntheses. All non-hydrogen atoms were refined with anisotropic displacement parameters. All hydrogen atom positions were found in the difference map calculated from the model containing all non-hydrogen atoms. The hydrogen positions were refined with individual isotropic displacement parameters. Full-matrix least-squares refinements with 285 parameters were carried out by minimizing $\sum w(F_o^2 - F_c^2)^2$ with SHELXL-97 weighting scheme and stopped at shift/err < 0.001. The final residual electron density maps showed no remarkable features. Neutral atom scattering factors for all atoms and anomalous dispersion corrections for the non-hydrogen atoms were taken from International Tables for Crystallography.^{46d} All calculations were performed on an Intel Pentium II PC, with the STRUX-V system, including the programs PLATON, SIR92 and SHELXL-97.⁴⁶

Compound 6. Crystal data and details of the structure determination are presented in Table 6. Suitable single crystals for the

X-ray diffraction study were grown from dichloromethane–diethyl ether (1 : 1). A dark green prism, was stored under perfluorinated ether, transferred in a Lindemann capillary, fixed and sealed. Preliminary examination and data collection were carried out on an area detecting system (STOE&Cie., IPDS I) at the window of a rotating anode (NONIUS, FR951) and graphite monochromated Mo-K α radiation ($\lambda = 0.71073$ Å). The unit cell parameters were obtained by full-matrix least-squares refinement of 1804 reflections. Data collection were performed at 293 K within a θ -range of $2.22 < \theta < 24.76^\circ$. One data set was measured in oscillation scan mode with $\Delta\phi = 1.0^\circ$. A total number of 12002 intensities were integrated. Raw data were corrected for Lorentz, polarization, and, arising from the scaling procedure, for latent decay and absorption effects. After merging ($R_{\text{int}} = 0.029$) a sum of 2984 (all data) and 2528 [$I > 2\sigma(I)$], respectively, remained and all data were used. The structure was solved by a combination of direct methods and difference Fourier syntheses. All non-hydrogen atoms were refined with anisotropic displacement parameters. All hydrogen atom positions were calculated in ideal positions (riding model). Full-matrix least-squares refinements with 244 parameters were carried out by minimizing $\sum w(F_o^2 - F_c^2)^2$ with SHELXL-97 weighting scheme and stopped at shift/err < 0.001. The final residual electron density maps showed no remarkable features. A disorder of the BF $_4$ -anion over two positions (0.50/0.50) could be resolved clearly. Neutral atom scattering factors for all atoms and anomalous dispersion corrections for the non-hydrogen atoms were taken from International Tables for Crystallography.^{46d} All calculations were performed on an Intel Pentium II PC, with the STRUX-V system, including the programs PLATON, SIR92 and SHELXL-97.⁴⁶

Computational details

DFT³⁹ calculations were performed using the GAUSSIAN 03 software package,⁴³ and the PBE1PBE functional, without symmetry constraints. That functional uses a hybrid generalised gradient approximation (GGA), including 25% mixture of Hartree–Fock⁴⁷ exchange with DFT³⁹ exchange–correlation, given by Perdew, Burke and Ernzerhof functional (PBE).⁴⁸ The optimised geometries were obtained with the LanL2DZ basis set⁴⁹ augmented with a f-polarization function⁵⁰ for Mo and a standard 6-31G(d,p)⁵¹ for the remaining elements. Transition state optimizations were performed with the synchronous transit-guided quasi-Newton method (STQN) developed by Schlegel *et al.*,⁵² after a thorough search of the potential energy surfaces (PES). Frequency calculations were performed to confirm the nature of the stationary points, yielding one imaginary frequency for the transition states and none for the minima. Each transition state was further confirmed by following its vibrational mode downhill on both sides, and obtaining the minima presented on the energy profiles.

The molecular dynamics simulations of the macrocycles were performed with the GROMOS 53A6 force field^{53,54} using GROMACS 4.5.1^{55,56} and with the SPC water model.⁵⁷ Periodic boundary conditions were used with rhombic dodecahedral unit cell. A twin-range cutoff was used, with short- and long-range cutoffs of 8 and 14 Å, respectively, and with neighbour lists updated every five steps. Long-range electrostatic interactions were treated with the reaction-field method^{58,59} using a dielectric constant of 54. The ligand was constrained using the LINCS

algorithm,⁶⁰ while the SETTLE algorithm was used for water.⁶¹ The time step used was 2 fs. The temperature of the ligands and water molecules were separately coupled to a Berendsen's temperature bath at 300 K and with relaxation times of 0.1 ps.⁶² A Berendsen's pressure coupling⁶² at 1 bar was used with a relaxation time of 0.5 ps and a compressibility of 4.5×10^{-5} bar $^{-1}$. The clustering analyses were performed using the GROMACS tool *g_cluster* and the Jarvis–Patrick clustering method with cutoffs of 0.06–0.08 nm.

Three-dimensional representations of structures were obtained with Chemcraft.⁶³

Acknowledgements

L. F. V. acknowledges UTL/Santander for partial funding. The NMR spectrometers are part of the National NMR Network and were purchased in the framework of the National Program for Scientific Re-equipment, contract REDE/1517/RMN/2005, with funds from POCI 2010 (FEDER) and Fundação para a Ciência e a Tecnologia (FCT).

References

- 1 J. M. O'Connor and C. P. Casey, *Chem. Rev.*, 1987, **87**, 307.
- 2 N. T. Anh, M. Elian and R. Hoffmann, *J. Am. Chem. Soc.*, 1978, **100**, 110.
- 3 A. J. Hart-Davis and R. J. Mawby, *J. Chem. Soc. A*, 1969, 2403.
- 4 C. White and R. J. Mawby, *Inorg. Chim. Acta*, 1970, **4**, 261.
- 5 A. J. Hart-Davis, C. White and R. J. Mawby, *Inorg. Chim. Acta*, 1970, **4**, 441.
- 6 D. J. Jones and R. J. Mawby, *Inorg. Chim. Acta*, 1972, **6**, 157.
- 7 M. E. Rerek, L.-N. Ji and F. Basolo, *J. Chem. Soc., Chem. Commun.*, 1983, 1208.
- 8 L.-N. Ji, M. E. Rerek and F. Basolo, *Organometallics*, 1984, **3**, 740.
- 9 M. E. Rerek and F. Basolo, *Organometallics*, 1983, **2**, 372.
- 10 (a) H. Bönemann, *Angew. Chem., Int. Ed. Engl.*, 1985, **24**, 248; (b) T. B. Marder, D. C. Roe and D. Milstein, *Organometallics*, 1988, **7**, 1451; (c) R. S. Tanke and R. H. Crabtree, *J. Am. Chem. Soc.*, 1990, **112**, 7984; (d) T. Foo and R. G. Bergman, *Organometallics*, 1992, **11**, 1801; (e) G. H. Llinas, R. O. Day, M. D. Rausch and J. C. W. Chien, *Organometallics*, 1993, **12**, 1283; (f) C. Bonifaci, A. Cecon, A. Gambaro, P. Ganis, L. Mantovani, S. Santi and A. Venzo, *J. Organomet. Chem.*, 1994, **475**, 267; (g) L. Mantovani, A. Cecon, A. Gambaro, S. Santi, P. Ganis and A. Venzo, *Organometallics*, 1997, **16**, 2682; (h) L. Orian, J. N. P. van Stralen and F. M. Bickelhaupt, *Organometallics*, 2007, **26**, 3816.
- 11 B. Y. Lee, Y. K. Chung, N. Jeong, Y. Lee and S. H. Hwang, *J. Am. Chem. Soc.*, 1994, **116**, 8793.
- 12 (a) C. E. Garrett and G. C. Fu, *J. Org. Chem.*, 1998, **63**, 1370; (b) C. N. Garon, D. I. McIsaac, C. M. Vogels, A. Decken, I. D. Williams, C. Kleeberg, T. B. Marder and S. A. Westcott, *Dalton Trans.*, 2009, 1624–1631.
- 13 (a) T. E. Ready, R. O. Day, J. C. W. Chien and M. D. Rausch, *Macromolecules*, 1993, **26**, 5822; (b) H. H. Brintzinger, D. Fischer, R. Mulhaupt, B. Rieger and R. M. Waymouth, *Angew. Chem., Int. Ed. Engl.*, 1995, **34**, 1143; (c) M. A. Schmid, H. G. Alt and W. Milius, *J. Organomet. Chem.*, 1996, **514**, 45; (d) A. L. McKnight and R. M. Waymouth, *Chem. Rev.*, 1998, **98**, 2587; (e) H. G. Alt and A. Koppl, *Chem. Rev.*, 2000, **100**, 1205; (f) G. W. Coates, *Chem. Rev.*, 2000, **100**, 1223; (g) S. Arndt and J. Okuda, *Chem. Rev.*, 2002, **102**, 1953; (h) L. Resconi, L. Cavallo, A. Fait and F. Piemontesi, *Chem. Rev.*, 2000, **100**, 1253.
- 14 (a) E. Kirilov, L. Toupet, C. W. Lehmann, A. Razavi, S. Kahlal, J.-Y. Saillard and J.-F. Carpentier, *Organometallics*, 2003, **22**, 4038; (b) E. Kirilov, C. W. Lehmann, A. Razavi and J.-F. Carpentier, *J. Am. Chem. Soc.*, 2004, **126**, 12240; (c) A.-S. Rodrigues, E. Kirilov, C. W. Lehmann, T. Roisnel, B. Vuillemin, A. Razavi and J.-F. Carpentier, *Chem.–Eur. J.*, 2007, **13**, 5548.
- 15 M. J. Calhorda, C. C. Romão and L. F. Veiros, *Chem.–Eur. J.*, 2002, **8**, 868.

- 16 (a) S. Brydges, N. Reginato, L. P. Cuffe, C. M. Seward and M. J. McGlinchey, *C. R. Chim.*, 2005, **8**, 1497; (b) E. Kirilov, S. Kahlal, T. Roisnel, T. Georgelin, J.-Y. Saillard and J.-F. Carpentier, *Organometallics*, 2008, **27**, 387.
- 17 (a) C. A. Bradley, L. F. Veiros, D. Pun, E. Lobkovsky, I. Keresztes and P. J. Chirik, *J. Am. Chem. Soc.*, 2006, **128**, 16600; (b) M. Prinz, L. F. Veiros, M. J. Calhorda, C. C. Romão, E. Herdtweck, F. E. Kühn and W. A. Herrmann, *J. Organomet. Chem.*, 2006, **691**, 4446.
- 18 K. Nikitin, H. Müller-Bunz, Y. Ortin and M. J. McGlinchey, *Chem.–Eur. J.*, 2009, **15**, 1836.
- 19 (a) S. Bordoni, S. Cerini, R. Tarroni, S. Zacchini and L. Busetto, *Organometallics*, 2009, **28**, 5382; (b) J. A. Crisp, R. M. Meier, J. S. Overby, T. P. Hanusa, A. L. Rheingold and W. W. Brennessel, *Organometallics*, 2010, **29**, 2322.
- 20 M. J. Calhorda and L. F. Veiros, *J. Organomet. Chem.*, 2001, **635**, 197.
- 21 M. E. Stoll, P. Belanzoni, M. J. Calhorda, M. G. B. Drew, V. Félix, W. E. Geiger, C. A. Gamelas, I. S. Gonçalves, C. C. Romão and L. F. Veiros, *J. Am. Chem. Soc.*, 2001, **123**, 10595.
- 22 S. Y. Ng, J. Tan, W. Y. Fan, W. K. Leong, L. Y. Goh and R. D. Webster, *Eur. J. Inorg. Chem.*, 2007, 3827.
- 23 H. Ahmed and J. E. McGrady, *J. Organomet. Chem.*, 2008, **693**, 3697.
- 24 P. Oulié, C. Freund, N. Saffon, B. Martin-Vaca, L. Maron and D. Bourissou, *Organometallics*, 2007, **26**, 6793.
- 25 S. Bordoni, S. Cerini, R. Tarroni, S. Zacchini and L. Busetto, *Organometallics*, 2009, **28**, 5382.
- 26 D. A. Kissounko, M. V. Zabalov, N. M. Boag, Y. F. Oprunenko and D. A. Lemenovskii, *J. Organomet. Chem.*, 2008, **693**, 1058.
- 27 H. Wang, Y. Xie, R. B. King and H. F. Schaefer III, *Eur. J. Inorg. Chem.*, 2008, 3698.
- 28 C. A. Bradley, E. Lobkovsky and P. J. Chirik, *J. Am. Chem. Soc.*, 2003, **125**, 8110.
- 29 C. A. Bradley, I. Keresztes, E. Lobkovsky, V. G. Young and P. J. Chirik, *J. Am. Chem. Soc.*, 2004, **126**, 16937.
- 30 L. F. Veiros, *Chem.–Eur. J.*, 2005, **11**, 2505.
- 31 L. F. Veiros and M. J. Calhorda, *Dalton Trans.*, 2011, DOI: 10.1039/C1DT00010A.
- 32 J. R. Ascenso, I. S. Gonçalves, E. Herdtweck and C. C. Romão, *J. Organomet. Chem.*, 1998, **508**, 169.
- 33 M. J. Calhorda, C. A. Gamelas, I. S. Gonçalves, E. Herdtweck, C. C. Romão and L. F. Veiros, *Organometallics*, 1998, **17**, 2597.
- 34 G. E. D. Mullen, M. J. Went, S. Wocadlo, A. K. Powell and P. J. Blower, *Angew. Chem., Int. Ed. Engl.*, 1997, **36**, 1205.
- 35 (a) M. A. Bennett, L. Y. Goh and A. C. Willis, *J. Chem. Soc., Chem. Commun.*, 1992, 1180; (b) A. J. Blake, A. J. Holder, T. I. Hyde, H.-J. Küppers, M. Schröder, S. Stötzl and K. Wieghardt, *J. Chem. Soc., Chem. Commun.*, 1989, 1600.
- 36 M. D. Curtis and S. H. Druker, *J. Am. Chem. Soc.*, 1997, **119**, 1027.
- 37 M. R. Du Bois, *Polyhedron*, 1997, **16**, 3089.
- 38 G. H. Spies and R. J. Angelici, *Organometallics*, 1987, **6**, 1897.
- 39 R. G. Parr and W. Yang, *Density Functional Theory of Atoms and Molecules*, Oxford University Press, New York, 1989.
- 40 J. W. Faller, R. H. Crabtree and A. Habib, *Organometallics*, 1985, **4**, 929.
- 41 (a) J. Markham, K. Menard and A. Cutler, *Inorg. Chem.*, 1985, **24**, 1581; (b) J. R. Ascenso, C. G. Azevedo, I. S. Gonçalves, E. Herdtweck, D. S. Moreno, C. C. Romão and J. Zühlke, *Organometallics*, 1994, **13**, 429; (c) J. R. Ascenso, C. G. Azevedo, I. S. Gonçalves, E. Herdtweck, D. S. Moreno, M. Pessanha and C. C. Romão, *Organometallics*, 1995, **14**, 3901; (d) I. S. Gonçalves and C. C. Romão, *J. Organomet. Chem.*, 1995, **486**, 155.
- 42 T. Yoshida, T. Adachi, K. Sato, K. Baba and T. Kanokogi, *J. Chem. Soc., Chem. Commun.*, 1993, 1511.
- 43 GAUSSIAN 03, Revision C.02, M. J. Frisch, G. W. Trucks, H. B. Schlegel, G. E. Scuseria, M. A. Robb, J. R. Cheeseman, J. A. Montgomery, Jr., T. Vreven, K. N. Kudin, J. C. Burant, J. M. Millam, S. S. Iyengar, J. Tomasi, V. Barone, B. Mennucci, M. Cossi, G. Scalmani, N. Rega, G. A. Petersson, H. Nakatsuji, M. Hada, M. Ehara, K. Toyota, R. Fukuda, J. Hasegawa, M. Ishida, T. Nakajima, Y. Honda, O. Kitao, H. Nakai, M. Klene, X. Li, J. E. Knox, H. P. Hratchian, J. B. Cross, C. Adamo, J. Jaramillo, R. Gomperts, R. E. Stratmann, O. Yazyev, A. J. Austin, R. Cammi, C. Pomelli, J. W. Ochterski, P. Y. Ayala, K. Morokuma, G. A. Voth, P. Salvador, J. J. Dannenberg, V. G. Zakrzewski, S. Dapprich, A. D. Daniels, M. C. Strain, O. Farkas, D. K. Malick, A. D. Rabuck, K. Raghavachari, J. B. Foresman, J. V. Ortiz, Q. Cui, A. G. Baboul, S. Clifford, J. Cioslowski, B. B. Stefanov, G. Liu, A. Liashenko, P. Piskorz, I. Komaromi, R. L. Martin, D. J. Fox, T. Keith, M. A. Al-Laham, C. Y. Peng, A. Nanayakkara, M. Challacombe, P. M. W. Gill, B. Johnson, W. Chen, M. W. Wong, C. Gonzalez and J. A. Pople, Gaussian, Inc., Wallingford CT, 2004.
- 44 J. Beech, P. J. Cragg and M. G. B. Drew, *J. Chem. Soc., Dalton Trans.*, 1994, 719.
- 45 A. Magistrato, P. Maurer, T. Fässler and U. Rothlisberger, *J. Phys. Chem. A*, 2004, **108**, 2008.
- 46 (a) *Data Collection Software for NONIUS κ -CCD devices*, Delft, The Netherlands, 1997; (b) *IPDS Operating System Version 2.2. STOE&CIE*, GmbH, Darmstadt, Germany, 1994; (c) Z. Otwinowski and W. Minor, *Methods Enzymol.*, 1997, **276**, 307; (d) *International Tables for Crystallography*, Vol. C, ed. Th. Hahn and A. J. C. Wilson, Kluwer Academic Publisher, Dordrecht, Boston, London, 3rd edn, 1992; (e) G. Artus, W. Scherer, T. Priermeier and E. Herdtweck, *STRUX-V: A Program System to Handle X-Ray Data*, TU München, Garching, Germany, 1997; (f) A. L. Spek, *PLATON: A Multipurpose Crystallographic Tool*, Utrecht University, Utrecht, The Netherlands, 2001; (g) A. Altomare, G. Casciaro, C. Giacovazzo, A. Guagliardi, M. C. Burla, G. Polidori and M. Camalli, *SIR92, J. Appl. Crystallogr.*, 1994, **27**, 435–436; (h) G. M. Sheldrick, *SHELXL-97*, University of Göttingen, Göttingen, Germany, 1998.
- 47 W. J. Hehre, L. Radom, P. v. R. Schleyer and J. A. Pople, *Ab Initio Molecular Orbital Theory*, John Wiley & Sons, NY, 1986.
- 48 (a) J. P. Perdew, K. Burke and M. Ernzerhof, *Phys. Rev. Lett.*, 1997, **78**, 1396; (b) J. P. Perdew, *Phys. Rev. B*, 1986, **33**, 8822.
- 49 (a) T. H. Dunning Jr. and P. J. Hay, *Modern Theoretical Chemistry*, ed. H. F. III Schaefer (Plenum, New York, 1976), vol. 3, p. 1; (b) P. J. Hay and W. R. Wadt, *J. Chem. Phys.*, 1985, **82**, 270; (c) W. R. Wadt and P. J. Hay, *J. Chem. Phys.*, 1985, **82**, 284; (d) P. J. Hay and W. R. Wadt, *J. Chem. Phys.*, 1985, **82**, 2299.
- 50 A. W. Ehlers, M. Böhme, S. Dapprich, A. Gobbi, A. Höllwarth, V. Jonas, K. F. Köhler, R. Stegmann, A. Veldkamp and G. Frenking, *Chem. Phys. Lett.*, 1993, **208**, 111.
- 51 (a) R. Ditchfield, W. J. Hehre and J. A. Pople, *J. Chem. Phys.*, 1971, **54**, 724; (b) W. J. Hehre, R. Ditchfield and J. A. Pople, *J. Chem. Phys.*, 1972, **56**, 2257; (c) P. C. Hariharan and J. A. Pople, *Mol. Phys.*, 1974, **27**, 209; (d) M. S. Gordon, *Chem. Phys. Lett.*, 1980, **76**, 163; (e) P. C. Hariharan and J. A. Pople, *Theor. Chim. Acta*, 1973, **28**, 213.
- 52 (a) C. Peng, P. Y. Ayala, H. B. Schlegel and M. J. Frisch, *J. Comput. Chem.*, 1996, **17**, 49; (b) C. Peng and H. B. Schlegel, *Isr. J. Chem.*, 1994, **33**, 449.
- 53 W. R. P. Scott, P. H. Hünenberger, I. G. Tironi, A. E. Mark, S. R. Biller, J. Fennen, A. E. Torda, T. Hüber, P. Kruger and W. F. J. van Gunsteren, *J. Phys. Chem. A*, 1999, **103**, 3596.
- 54 C. Oostenbrink, A. Villa, A. E. Mark and W. F. J. van Gunsteren, *J. Comput. Chem.*, 2004, **25**, 1656.
- 55 H. J. C. Berendsen, D. van der Spoel and R. van Drunen, *Comput. Phys. Commun.*, 1995, **91**, 43.
- 56 B. Hess, C. Kutzner, D. van der Spoel and E. J. Lindahl, *J. Chem. Theory Comput.*, 2008, **4**, 435.
- 57 J. Hermans, H. J. C. Berendsen, W. F. van Gunsteren and J. P. M. Postma, *Biopolymers*, 1984, **23**, 1513.
- 58 J. A. Barker and R. O. Watts, *Mol. Phys.*, 1973, **26**, 789.
- 59 I. G. Tironi, R. Sperb, P. E. Smith and W. F. J. van Gunsteren, *Chem. Phys.*, 1995, **102**, 5451.
- 60 B. Hess, H. Bekker, H. J. C. Berendsen and J. G. E. M. Fraaije, *J. Comput. Chem.*, 1997, **18**, 1463.
- 61 S. Miyamoto and P. A. Kollman, *J. Comput. Chem.*, 1992, **13**, 952.
- 62 H. J. C. Berendsen, J. P. M. Postma, W. F. van Gunsteren, A. Dinola and J. R. Haak, *J. Chem. Phys.*, 1984, **81**, 3684.
- 63 <http://www.chemcraftprog.com/index.html>.